




Cite this: *Sustainable Energy Fuels*,
2025, 9, 2433

Energy-environmental analysis of an H₂PEM power station assisted by a dynamic simulation tool

Orlando Corigliano * and Petronilla Fragiaco

This paper reports on the development of a numerical tool tailored to perform energy and environmental analyses for an H₂PEM power station, comprising fuel cell and electrolysis units, with a dual-mechanism H₂ storage that incorporates compression and metal hydride tanks. A comprehensive methodology for the design, modeling, and simulation is introduced, focusing on the interaction of the H₂PEM with a higher-level network that exchanges electrical power. The H₂PEM is 1 kW level, with a H₂ storage capacity of 5 Nm³. The work stands out for the modeling of subsystem interconnections under a strategic operational plan, offering an integrated understanding of system behavior. The modeling includes temperature regulation, encompassing the assessment of heat management, as well as that of the auxiliaries. Steady state and dynamic simulations are conducted within the Matlab/Simulink computational environment to assess the performance under various conditions. The energy and environmental analyses comprise determining key parameters such as involved energies, hydrogen production and consumption, state of charge of the hydrogen reservoir, CO₂ emissions and savings, and associated temperature changes. Three case scenarios are assessed, considering H₂PEM interacting with a network powered by: (1) solely fossil-based electricity, (2) the Italian energy mix for 2023, and (3) entirely renewable energy sources. Results revealed nominal efficiency of 55% for the electrolyzer and 40.5% for fuel cell. About 1 order of magnitude of CO₂ is saved when the H₂PEM is totally renewable (93.36 vs. 1.539 kg_{CO₂} kg_{H₂}⁻¹). The temperature increase associated is 10.5 × 10⁻³ °C per ppm of CO₂ emitted.

Received 18th February 2025
Accepted 13th March 2025

DOI: 10.1039/d5se00257e

rsc.li/sustainable-energy

Introduction

The global race towards energy transition to enhance energy efficiency, mitigate climate change and environmental pollution is increasingly centered around hydrogen energy.^{1–7} On 8th July 2020, the European Commission unveiled “A hydrogen strategy for a climate-neutral Europe”, outlining a collective European approach to promote hydrogen utilization.^{8–10} The strategy aims to deploy a minimum of 40 GW of electrolyzers by 2030 and produce up to 10 million tonnes of renewable hydrogen within the European Union. Alongside this strategic plan, the European Clean Hydrogen Alliance¹¹ was introduced, serving as a collaborative platform for industry, national and local authorities, civil society, and all stakeholders involved in establishing a comprehensive and efficient European green hydrogen supply chain.

Hydrogen plays a pivotal role in the energy transition by offering a versatile and clean fuel alternative that aligns closely with the United Nations Sustainable Development Goals (SDGs).¹² Specifically, hydrogen supports SDG 7 (Affordable and Clean Energy) by enabling the production of energy from

diverse, renewable sources such as wind, solar, and hydro, thereby reducing dependency on fossil fuels and enhancing energy security. Additionally, hydrogen technology contributes to SDG 13 (Climate Action) by significantly lowering greenhouse gas emissions.

Hydrogen is increasingly regarded as a key solution for “hard-to-abate” sectors, with its use primarily linked to fuel cells for energy generation. In this context, water is the only byproduct, significantly reducing carbon footprints and contributing to climate change mitigation. Hydrogen can be produced through various methods and technologies, ranging from thermochemical processes¹³ such as reforming, bio-gasification, and hydrocarbon cracking, to purely electrochemical techniques.¹⁴ Among these, electrolysis powered by renewable energy sources is considered the cleanest and most environmentally friendly approach.

This elucidates the rationale behind the substantial interest surrounding electrochemical devices within the scientific and industrial landscape of clean hydrogen energy.^{1,15–19} Significant benefits arise from the widespread adoption of hydrogen systems, including reduced fossil fuel consumption, lower CO₂ emissions, and enhanced public health. These advantages are closely aligned with ongoing technological advancements and supportive policy frameworks.

Department of Mechanical, Energy and Management Engineering, University of Calabria, Arcavacata di Rende, Cosenza, Italy. E-mail: orlando.corigliano@unical.it; petronilla.fragiacomo@unical.it



To achieve net-zero emissions by 2050, the deployed capacity of electrolysis must reach nearly 3600 GW.²⁰ Several initiatives and government incentives are actively supporting this goal. Additionally, electrolytic hydrogen production is encouraged to generate other medium fuels, referred to as e-fuels, such as ammonia, methane, and methanol. These fuels are valuable not only for their direct applications but also as hydrogen carriers.²¹ Numerous projects are currently underway. In this context, Fig. 1 shows a map of announced low-emission hydrogen production projects set for 2024, based on the IEA's 'Global Hydrogen Review 2024' report.²²

Government initiatives, including carbon pricing and subsidies for low-carbon technologies, play a crucial role in bridging the cost gap between hydrogen and fossil fuels. For instance, implementing a carbon price of \$50 per ton of CO₂ could significantly improve the economic viability of hydrogen systems.²³ Educational programs aimed at increasing public awareness and reducing skepticism are equally essential for accelerating the adoption of hydrogen technologies.

Integrating hydrogen energy systems with renewable sources like solar and wind presents a valuable opportunity to stabilize and diversify energy supplies. Hydrogen produced through Power-to-Gas (P2G) technology can even be mixed with natural gas within existing infrastructure, enabling its use in power generation, transportation, and heating with minimal modifications to current systems.²⁴

PEM technology for electrolysis and fuel cells

Electrolyzers and fuel cells using Polymer Electrolyte Membrane (PEM) have now gained a certain degree of technological maturity.^{25–32} The PEM technology exhibits several advantages. High power density, fast response times, and compact designs are some of the benefits, to which a high level of safety and social acceptance is added.^{33–38} PEM electrolyzers (PEMEL) produce high-purity hydrogen and facilitate the utilization of surplus renewable energy by converting it into storable hydrogen, thus contributing to grid stability and the utilization of intermittent renewable source.^{39,40} PEM fuel cells (PEMFC) are well-suited for applications in stationary power generation, transportation and even portable electronic devices.^{41–44} Pure hydrogen feeding

attributes to PEMFCs the great benefit deriving by clean and emissions-free energy conversion process.

However, challenges remain in the widespread deployment of PEMELs and PEMFCs, such as cost reduction, durability improvements, and scaling up production.^{2,4,8} Additionally, targets are aimed to enhance the overall system efficiency^{9,10,45,46} through innovative design and manufacturing approaches,^{30,47–49} integration of advanced materials,^{28,30} alternative and cheaper catalyst materials.^{46,47,50–52}

These devices are modular in design, which facilitates the assembly of large-scale systems by connecting multiple modules. Regarding technical scalability, to meet large-scale industrial demands, PEM electrolyzers can be configured in units up to 10 MW, with projects like REFHYNE II† targeting capacities of 100 MW or more. The Hysencia project,‡ for example, incorporates a 35 MW electrolyzer paired with a 49 MWp solar photovoltaic plant, providing significant renewable electricity annually to power the electrolyzer. Additionally, Cummins Technology's HyLYZER® 4000-30 has an installed capacity of 20 MW. According to Wappler *et al.*,⁵³ the potential installed capacity of electrolyzers could reach 900 GW by 2030, which would lead to a rapid reduction in costs due to economies of scale and could reduce greenhouse gas emissions by up to 830 million tons of CO₂ annually.²³ PEM fuel cell systems also demonstrate significant scalability, as outlined in the SRIA report.¹⁰ The manufacturing capacity for single PEMFC systems ranges from below 5 kW to 500 kW, suggesting the potential for widespread deployment at the decentralized level. Plug Power commercializes PEM fuel cell systems up to 1 MW, based on arrays of 125 kW ProGen§ modules. Projections for 2030 suggest significant advancements in several areas.¹⁰ The energy consumption of PEM electrolyzers (PEMEL) is expected to decrease from 55 to 48 kW h kg^{−1}, while the initial capital expenditure (CAPEX) is projected to drop from 2100 € per kW to 1000 € per kW. Additionally, the degradation rate is anticipated to improve, decreasing from 0.19 to 0.12% per 1000 operating hours. For PEM fuel cells (PEMFCs), the CAPEX is also expected to decrease, with the possibility of halving for larger systems. The electric efficiency of PEMFCs is forecasted to increase from 45 to 56% by 2030. The durability of PEMFCs will also improve, with the degradation rate projected to decline from 0.4% per 1000 operating hours to 0.2% by 2030. In terms of hydrogen production costs from electrolysis, these are expected to fall from 5.3 € per kg in 2020 to 4.4 € per kg in 2030, and further to 2.7 € per kg by 2050. Moreover, hydrogen production costs in Asia could potentially drop to as low as 1.8 € per kg.⁵⁴

Hydrogen storage technologies

Production and use of hydrogen cannot be separated from the concept of storage,⁵⁵ crucial for supporting a wide range of applications, including transportation, power generation,

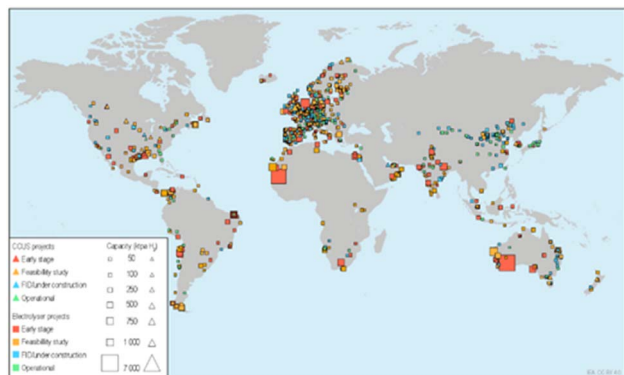


Fig. 1 Map of announced low-emissions hydrogen production projects, 2024.²²

† <https://www.refhyne.eu/refhyne-2/>.

‡ <https://dh2energy.com/en/projects/>.

§ <https://www.plugpower.com/fuel-cell-power/gensure-stationary-power-systems/gensure-mw-scale-power/>.



Table 1 Energy requirements for different hydrogen storage methods

Energy expenditure				
Storage	Notes	Storing H ₂ [kJ kg ⁻¹]	Releasing H ₂ [kJ kg ⁻¹]	Energy ratio $\varepsilon = \frac{E_{\text{spent}}}{E_{\text{stroed}}}$
Compression	20 MPa	10 300	0	0.09
	35 MPa	12 264	0	0.10
	70 MPa	14 883	0	0.12
Liquefaction	Liquid	42 600	0	0.36
Metal hydrides	15–30	6226–10 865	1071–6724	0.06–0.15
Ammonia	Liquid	6900	17 670	1.16
Hydrate-based		11 215	0	0.09

distribution and industrial processes.⁵⁶ Hydrogen storage technology can be classified according to physical and material-based technologies.^{57,58} Compressed gas, liquid form and cryo-compressed form are included in the physical-based methods. Material-based methods, also known as solid-state storage, involve sorption and desorption techniques.

Compressed gas storage involves storing hydrogen at high pressures, typically in reinforced tanks (Type I–V). Liquid hydrogen storage involves cooling hydrogen to extremely low temperatures, allowing it to be stored as a liquid. Solid-state storage methods utilize materials such as metal hydrides, carbon nanotubes, or porous structures to absorb and release hydrogen. Chemical storage involves chemically binding hydrogen to specific compounds, such as chemical carriers, which can release hydrogen through specific reactions. Currently, the metal hydride-based storage system is gaining considerable interest. This approach is highly regarded for its high safety standards, stemming from the ability to efficiently store hydrogen at low pressures and temperatures. In summary, compressed gas storage of hydrogen in aboveground pressure vessels up to 1000 bar is suitable for small to medium-scale applications. For large-scale and long-term storage, salt caves are being considered.⁵⁹ Liquid hydrogen systems are primarily used when high storage capacity is necessary,⁶⁰ as for aviation purposes. Chemical storage using ammonia is an attractive option as it offers a high hydrogen storage density of 17.8 weight percent (wt%) or 10.7 kg of H₂ per 100 liters. Additionally, ammonia can be easily liquefied.⁶¹ Hydride storage has notable advantages, as it can accumulate comparable or even greater amounts of hydrogen at relatively low pressures, making it more socially acceptable. This technology can achieve an energy density of approximately 5 kW h_{H₂} l⁻¹, which is up to three times higher than the physical storage system at 700 bar.⁶² Various metals such as magnesium (Mg), sodium (Na), lithium (Li), calcium (Ca), and aluminium (Al) show promise as candidates for hydrogen storage. Sodium borohydride-based tanks, for example, offer hydrogen storage capacities of around 10.7 wt% or 5.72 kg of H₂ per 100 liters (1.3 wt% or 0.5 kg_{H₂}/100 l considering the entire system).^{63–66}

Aboveground storage tanks are projected to have a capital cost of 600 € per kg, and storage capacity is set to increase from the current 1.1 ton to 20 tons, with a storage density exceeding 40 kg of hydrogen per cubic meter of storage vessel. For more

detailed information, refer to ref. 4. This review analysis is summarized in Table 1, reporting the energy requirements for different hydrogen storage methods.^{67,68}

Metal hydrides represent one of the best energy storage options, as they exhibit the lowest energy expenditure-to-storage ratio. It is important to note that metal hydride systems require cooling for hydrogen charging and heat for hydrogen release. In the case of ammonia, the storage phase involves the conversion of hydrogen into the e-fuel, which is exothermic. However, the release phase requires energy for the reconversion of hydrogen, as this process is endothermic.

The subsequent paragraph provides an overview of the current state of modeling activities documented in the scientific literature.

Literature background on system modeling

The mathematical modeling is fundamental for understanding performance, critical issues and limitations, optimizing system design, and predicting behavior under various operating conditions, as well as facilitating scale-up of systems.

The scientific literature presents a substantial body of work focused on numerical modeling activities related to PEMEL, PEMFC, and hydrogen storage. Numerous review papers continuously emerge, aiming to update modeling techniques in line with technological advancements in these devices.^{69–78} By employing diverse keywords in prominent bibliographic search engines, researchers can access a vast array of pertinent results, extending into the thousands. Models of varying complexities are available, including those based on empirical,^{79–86} semi-empirical,^{87–93} and mechanistic^{78,94–98} methods.

In order to comprehensively analyze the design of PEMEL and PEMFC, models encompassing thermal-flow distributions and energy performance can be developed at different levels of complexity, spanning from lumped parameter or 0-dimensional (0-D) models to 1-dimensional (1-D), 2-dimensional (2-D), and 3-dimensional (3-D) models. While 1-D and 2-D models offer detailed characterization of physical processes, 3-D models provide a comprehensive representation of the components and the entire system. It is important to distinguish between modeling at the cell/stack level and at the Balance of Plant (BoP) level. In the latter case, the performance investigation serves as a guide for designing the entire system and simulating its



behavior under various operating conditions. The utilization of 0-D modeling is particularly relevant when focusing on BoP considerations.

Modeling approaches in this context can also be categorized as steady-state and dynamic.^{94,99–101} Steady-state models assume that all state variables remain stable locally and offer a comprehensive evaluation of cell and stack performance under steady operating conditions. On the other hand, dynamic models capture transient behavior by simulating changes uncertain operating conditions, allowing for a detailed analysis of system response to fluctuations and dynamic processes.

Without going into excessive details of the modeling of transport and/or electrochemical phenomena, since this is not the scope of this work, the investigation is concentrated on the papers dealing with system-level modeling with particular reference to integrated energy systems with hydrogen accumulation for exchanges of energy flows with external energy networks.

The bibliographic search employed specific keywords and key phrases to identify the most relevant papers for the study. The selected terms included “PEM electrolyzer and fuel cell modeling in integrated energy systems with hydrogen accumulation for exchanges of energy flows with external energy networks”. By utilizing these targeted search parameters, an attempt was made to achieve a narrow focus, leading to the selection of about 30 recent papers deemed worthy of thorough investigation. This selection allowed valuable insights to be gained into the current state of modeling and numerical analysis in this particular field.

Shapiro *et al.* in 2005¹⁰² contributed a paper in which they presented a system proposal PV-PEMEL-high-pressure hydrogen and oxygen storage-PEMFC, in a closed water loop, furnishing data about the intersection between PV current and PEMEL current. Ferrero and Santarelli¹⁰³ developed a 2D finite element model for a high-pressure PEM water electrolyzer coupled with a photovoltaic multi-junction solar cell installed in a solar concentrator. The authors analyzed the thermo-electrochemical performance of the PEMEL, concluding that the coupling enhanced the performance. Ulleberg *et al.*¹⁰⁴ evaluated the performance of an autonomous wind/hydrogen energy demonstration system located on the island of Utsira, Norway. They employed a set of updated hydrogen energy system modeling tools (HYDROGEMS), specifically developed for TRNSYS16. The energy plant consists of a wind turbine (600 kW), a water electrolyzer ($10 \text{ Nm}^3 \text{ h}^{-1}$), hydrogen gas storage (2400 Nm^3 , 200 bar), a hydrogen engine (55 kW), a PEM fuel cell (10 kW), along with other auxiliary components. The tool allows to use a library with empirical relationships for current–voltage characteristics for solar cells or electrochemical cells and other equipment. Gallardo *et al.*¹⁰⁵ proposed a methodology to perform optimal sizing of AC-linked solar PV-PEMEL systems for hydrogen production. They used empirical equations and Black box for the PEMEL system model functional to perform multiyear simulations. Nsour *et al.*¹⁰⁶ presented a design of stand-alone PV-PEMEL-PEMFC system using HOMER, a computer model that simplifies the task of designing hybrid renewable micro-grids. Caparrós Mancera *et al.*¹⁰⁷ developed the

design, implementation, and practical experimentation of a BoP for a 4.5 kW_{el} PEMEL, with a control logic to guarantee efficient and safe operation. The authors presented a maximum efficiency of higher than 50%. Gracia *et al.*¹⁰⁸ presented a business case for off-grid hydrogen production *via* electrolysis, applied to the electrification of isolated sites, using the ODYSSEY tool (a proprietary tool developed by CEA-LITEN). This tool serves as an optimization platform for conducting comprehensive techno-economic assessments of energy systems, integrating renewable energy sources and energy storage units. Möller and Krauter^{109,110} presented a model of a hybrid energy and storage system based on photovoltaics coupled with lithium-ion battery and hydrogen generator using MATLAB/Simulink and HOMER, with an electrolyzer modeling. De Lorenzo *et al.*¹¹¹ developed dynamic electric simulation model for a PEMEL system coupled with a hydrogen storage. The authors developed a modeling in Matlab/Simulink environment with a special dedication on power converter aimed at receiving the external electric power. The objective was that of assessing PEMEL and storage performance at varying conditions. Zhang *et al.*¹¹² investigated the mechanism of cross-energy-form dynamic coupling, and proposed critical techniques of multienergy hybrid simulation. Saedi *et al.*¹¹³ presented a novel IEGS a modeling aimed at green hydrogen injections in the gas network by absorbing the variability of the renewables into electrolyzers. The gas system is modelled as a steady-state optimal gas flow. Pan *et al.*¹¹⁴ proposed an electricity hydrogen-integrated energy system planning model with the aim to plan electricity production and power to hydrogen and heat by occurrence. Boulmrharj *et al.*¹¹⁵ presented the performance assessment for a hybrid system with a hydrogen storage composed of PV-PEMEL-PEMFC. The modeling is developed on simplified assumption that rapidly allow to assess energy parameters necessary at investigating electricity and heat delivery for buildings. A 900 W electrolyzer and a 1200 W fuel cell are used in the analysis. Fan *et al.*¹¹⁶ developed a energy, exergy, and economic modeling, then the optimization of a flash-binary geothermal system aimed at power and hydrogen production using PEMEL. The authors assessed an overall power of about 115 kW and a hydrogen production capacity of 0.306 kg h^{-1} . For what regards the PEMEL a steady state approach was used. Ceylan *et al.*¹¹⁷ contributed a paper proposing the design and simulation of the PV/PEM fuel cell using MATLAB/Simulink. The authors subsequently extended the calculation in using a PEMEL for hydrogen production. In the latter case they used an empirical equation for the hydrogen mass flow rate as a function of surplus electric power. In general, modeling is approached by steady state modalities. Hai *et al.*¹¹⁸ modeled and examined transiently a variegated energy system with hydrogen generation, which include alkaline and proton exchange membrane electrolyzers, as well as heating and cooling systems. TRNSYS software was used from a thermodynamic and environmental point of view. No details are given on how hydrogen generation is modeled. Alirahmi *et al.*¹¹⁹ presented a comprehensive energy, exergy, and economic evaluations and optimizations of an integrated fuel cell/geothermal energy system for cooling and electricity. The simulations are



conducted using Engineering Equation Solver software, while a multi-objective optimization method is applied in MATLAB. A steady state approach was used in the simulations. Fărcaș *et al.*¹²⁰ presented a design and control method for PEM electrolyzer and hydrogen storage system. A simplified model is implemented for PEMEL in Matlab/Simulink environment. In the paper of Rostami *et al.*¹²¹ a solar driven-polygeneration energy system with electrical energy storage is investigated. An organic Rankine cycle is used to electrify an electrolyzer, whose H₂ and O₂ byproducts are subsequently used to power a fuel cell. A simplified steady state approach is used to model electrochemical devices. The authors declared a system efficiency of about 60%. Gonzatti *et al.*¹²² contributed an interesting review paper that adds the landscape of reviews in the field of modeling. The paper showcased a wide set of physic-chemical equations that integrate a large number of parameters and variables. Particular attention is dedicated to the storage system based on hydride metal tank, thus presenting absorption and desorption equations. Ganguly *et al.*¹²³ modeled and analyzed a 3.3 kW electrolyzer and two 480 W PEM fuel cell stacks in order to meet the power requirements of a 90 m² floriculture greenhouse, having as primary energy source a photovoltaic plant. The modeling was approached by a steady state typology and implemented *via* computer codes using 'C' language. Yelegen *et al.*¹²⁴ developed a 3-D two phase flow modeling of regenerative PEMFC. The modeling was applied to electro-cell with a 5 cm² active area. Pressure and velocity distribution were assessed along the electrode planes, and *I*-*V* curves both for electrolyzer and fuel cell were built under various temperatures. Experimental activity was conducted parallel to numerical one. 0.019 Sl min⁻¹ of hydrogen and 0.0095 Sl min⁻¹ of oxygen gas was produced in the electrolyzer mode, while a power density of 0.353 W cm⁻² was obtained in the fuel cell mode. Tao *et al.*¹²⁵ investigated an organic Rankine cycle coupled with a PEM electrolyzer, PEM fuel cell, and thermo-electric generator. The authors analyzed the system from technical and economical viewpoints, declaring to assess an energy efficiency of 16.77%, with a production of hydrogen of 0.0001632 mol h⁻¹. No details on fuel cell are described in the paper, as being referred to two bibliographic papers. No clear information can be drawn about hydrogen generation. Mohammadi *et al.*¹²⁶ illustrated an integrated energy system for clean and sustainable power functional to building applications. The system uses a PEM fuel cell fed with hydrogen derived by syngas. The system is examined from a technological, economic, and environmental aspect, while a multi-criteria optimization is employed to search for the lowest cost and emission as well as higher efficiency of the system. One valuable outcome outlined the net energy efficiency of the system of around 37.65%, employing a 5.04 MW PEM-FC. A semi-empirical approach for fuel cell was used. Chadly *et al.*¹²⁷ proposed a techno-economic analysis for an energy system varying on three layout scenarios. The paper compares three energy storage system technologies namely lithium-ion batteries, PEM reversible fuel cells and reversible solid oxide cells, with a stand-alone photovoltaic system. Zooming on reversible PEM fuel cell/electrolyzer results, a stack power of

about 250 kW for fuel cell and 590 kW for electrolyzer were deduced for the purpose, with a net efficiency of respectively about 50% and 77%, while a total system efficiency of about 38%. The results indicated a Levelized Cost of Storage of 41.42€ per kW per h. Sun *et al.*¹²⁸ proposed and investigated a solar-based CCHP unit, comprising of a solar-geothermal driven PEM electrolyzer in integration with Kalina cycle, absorption refrigeration cycle, and reverse osmosis. A non-dimension model was developed and a multi-criterial optimization process was employed from exergetic, energetic and exergo-economic standpoints. The analyses were conducted using a combination of Minitab and engineering equation solver. No equations are illustrated for what regards the electrolyzer and understand the detail of its modeling. The optimized condition expresses a unit cost of products and exergy performance of 1.7552 \$ per GJ and 31.7133%. Calise *et al.*¹²⁹ contributed a paper presenting a dynamic simulation model of a poly-generation system based on solar heating and cooling and PEM technologies. The analysis was carried out by means of a transient simulation model, developed using TRNSYS software and included the investigation of the dynamic behavior of the case study-building, developed in TRNBUILD. A 360 kW_e PEM fuel cell, with 34% of net efficiency was considered. Hydrogen and oxygen partial pressures at the Three Phase Boundary are calculated by empirical equations. The paper authored by Persson *et al.*¹³⁰ described the development of a semi-empirical model for an electrolyzer, utilizing real data obtained from a commercial electrolyzer. The essential data required for the model are the energy consumption and hydrogen production of the electrolyzer. Meanwhile, the article by Koundi *et al.*⁸⁵ focused on various components of a hydrogen production system based on PEM electrolyzer, including DC/DC power converters and control methods. The authors conducted a comprehensive review of the reference literature, examining the current state of PEM electrical modeling. The review encompasses empirical and semi-empirical models, both static and dynamic, shedding light on the advancements in this field. In a different study, Boulmrharj *et al.*¹³¹ presented their research on evaluating the performance of a hybrid system combining an electrolyzer, fuel cells, and hydrogen storage, designed for cogeneration in buildings. The paper outlines the modeling work, simulations, experiments, and performance evaluation of this innovative hybrid system, utilizing a photovoltaic plant as the primary source of renewable energy for hydrogen production. Still, the study of Chisatz *et al.*¹³² presented a thermodynamic and exergo-economic assessment of a proton exchange membrane fuel cell system at steady-state operations, finding an energy efficiency of the of 36.7% as the highest. Calise *et al.*¹³³ performed dynamic modeling and simulation using TRNSYS software package and economic analysis, finding a fuel cell electrical efficiency of 35%. The article of Kalinci *et al.* performed energy and exergy analyses of a hybrid hydrogen energy system, finding an efficiency of the electrolyzer of 59.68%.¹³⁴ Instead, study¹³⁵ introduced a computational algorithm designed to model an integrated photovoltaic-electrolysis-battery system. This work focused on optimizing both the cost of the system and its hydrogen production rate.



Discussion on literature and work contribution

From investigating the literature on PEM-based hydrogen storage energy systems, it can be deduced (to the best of the authors' knowledge) that this area is still susceptible to more in-depth exploration. Integrated systems and mixed technology hydrogen storage systems have not been fully modelled. Mixed storage technologies have not been employed in conjunction with each other. The examination of the selected papers has revealed the utilization of models incorporating simplified methodologies, black box techniques, and device-specific equations, especially at system level (for instance^{136–138}). Additionally, when investigating multi-objective optimization models, simplified fuel cell and electrolyzer approaches are usually adopted, leveraging straightforward empirical equations.

This work presents a numerical tool designed for conducting energy and environmental analyses of a hydrogen power station, here referred as H2PEM. This system includes a PEMFC and PEMEL, along with a dual-mechanism hydrogen storage system featuring both compression and metal hydride tanks. The tool, developed within the Matlab/Simulink computational environment, is suitable for both on-grid and off-grid applications.

This scientific endeavor stands out for its commitment to precision and a comprehensive approach. A distinctive aspect is the detailed attention to the interconnections between subsystems. This approach not only enhances the realism and applicability of the model but also contributes to a more integrated and holistic understanding of the system's behavior. The work describes each component of the balance of plant for subsystems, such as electrolysis and fuel cell units, using the governing equations that dictate their operation. This approach extends beyond the black-box one, up to include the auxiliary systems integral to the operation of these technologies. This allows for offering a level of detail and accuracy not commonly found in the field.

A lumped parameter model with a dynamic calculation function, calibrated and validated, forms the core of the

numerical tool. This choice is appropriate, as the objective of this work is to analyze the system at a holistic level, while capturing transient behavior in response to fluctuations and dynamic processes. This tool enables a thorough technical, energy, and environmental analysis. It calculates various aspects including energy involvement, hydrogen production and usage, the state of charge of the hydrogen reservoir. The energy mapping of the H2PEM system is then conducted under a range of operating conditions. From an environmental perspective, the analysis estimates CO₂ emissions and savings, as well as the associated temperature increase due to climate change, under three different scenarios. These scenarios consider the H2PEM interacting with a network powered by: (1) solely fossil-based electricity, (2) the Italian energy mix for 2023, and (3) entirely renewable energy sources. The Fig. 2 illustrates the work path of the paper.

Impacts, challenges and applications of hydrogen systems

Hydrogen systems are gaining increasing attention for their role in enhancing grid stability and supporting the transition to renewable energy sources.¹³⁹ These integrated systems leverage the complementary capabilities of PEM fuel cells and electrolyzers to manage fluctuations in power generation and consumption, thereby contributing to more resilient and sustainable energy grids.¹⁴⁰ Hydrogen storage plays a crucial role in this process by storing surplus energy as hydrogen, mitigating the effects of low renewable output periods.¹⁴¹

Nonetheless, hydrogen systems face a number of technical, durability, and economic challenges that must be overcome to ensure their widespread deployment. The barriers faced underscore the need for continued research and development efforts aimed at improving efficiency, reducing costs, and enhancing the durability and scalability of these systems. The following lines briefly (since this article is not focused on this topic) illustrate the main problems of hydrogen systems. For instance, electrodes in PEM fuel cells and electrolyzers can be subjected to degradation due to possible corrosive environments.^{142,143} This could lead to a reduction in efficiency and

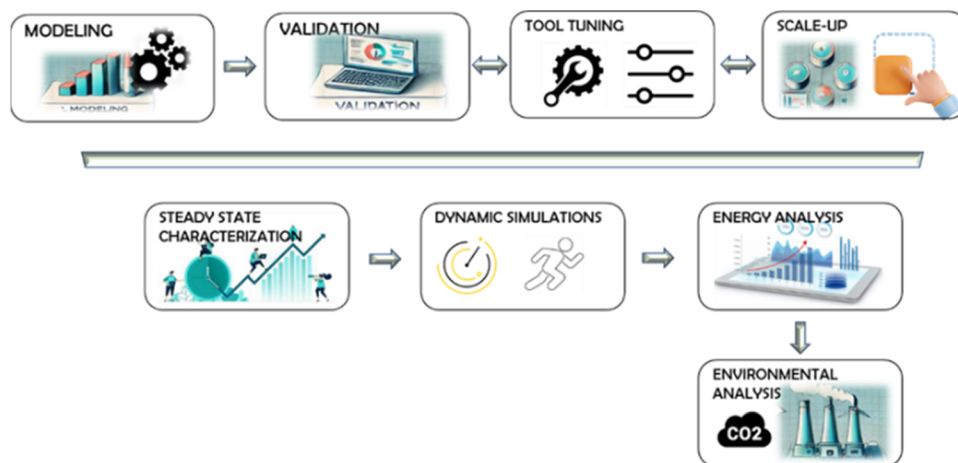


Fig. 2 Work path.



lifespan.¹⁴² As a consequence, degraded electrodes require frequent replacement, thus adding to the operational cost and limiting devices' long-term performance. Similarly applies to the proton exchange membrane (typically Nafion), it degrades over time due to oxidative attack, mechanical stress, and chemical reactions in the fuel cell's harsh environment.^{144,145} This could make arise the bottleneck increasing the internal resistance of the fuel cell, which reduces its efficiency and overall output.¹⁴² As a consequence, membrane replacement is costly and reduces the overall lifespan of the fuel cell. According to,¹⁴⁶ the lifespan of a PEMFC is expected to be on average at around 40 000 h, while study¹⁴⁷ considers a lifetime typically of 40 000–60 000 h for PEMEL commercial systems. From an economic perspective, the high initial cost (see paragraph "PEM technology for electrolysis and fuel cells") is primarily dependant of platinum-based catalysts and the complexity of manufacturing PEM devices fuel. About the storage (see paragraph "Hydrogen storage technologies"), the main challenge regards the storage capacity. Using conventional compression system, extremely high pressures are required. Furthermore, the compression tanks can suffer mechanical stresses like fatigue and other problems.¹⁴⁸ Fortunately, liquid and metal hydride technologies address these challenges, improving safety issues and social acceptability. Attention is dedicated to thermal management of metal hydride storage, in order to enhance the phase of absorption and desorption of hydrogen.¹⁴⁹ The bottleneck could be the high current cost due to young technology and not yet widely spread.

Regarding the integrated technologies in a system concept, recent technological advancements have focused on improving the efficiency and scalability of these systems. Advanced control algorithms and real-time data analytics are essential for optimizing system responsiveness to grid fluctuations and enhancing the efficiency of conversion devices,¹⁵⁰ as approximately 60% of incoming electricity is lost in conversion to hydrogen.¹⁵¹

In practical deployments, systems like "Energiepark Mainz" in Germany convert excess wind power into hydrogen, which is then used to generate electricity during low wind periods.¹⁵² Similarly, the HAEOLUS[¶] project integrates a 2.5 MW PEMEL in a remote Norwegian wind farm, converting collected wind energy into hydrogen with a 100 kW PEMFC.¹⁵³ In the telecommunications sector, H2PEM systems have shown promise. Telecom towers, which consume hundreds to thousands of kWh per month, are under pressure to reduce their carbon footprint due to rising energy demand.¹⁵⁴ Hydrogen fuel cell systems have proven effective in powering these towers, offering advantages over traditional backup power solutions.¹⁵⁵ Study¹⁵⁶ highlighted the competitiveness of hybrid renewable energy systems over traditional diesel generators at off-grid telecom stations, while study¹⁵⁷ demonstrated that slightly increasing the size of photovoltaic systems could reduce fossil fuel usage by 20%, lowering the Levelized Cost of Energy (LCOE) to 0.5 ± 0.1 € per kW per h.

The paper of Aliberti *et al.*¹⁵⁸ proposed methods for designing power supply systems for hydrogen-based telecom towers, optimizing component sizing and ensuring grid connectivity. Their work found that optimizing the system configuration could reduce both the simple payback (SPB) and LCOE by approximately 25 years and €0.30 kW h⁻¹, respectively, while halving the initial investment costs compared to islanded configurations. Further applications include hybrid renewable stations designed for power supply during grid outages. For example, Zhang *et al.*¹⁵⁹ proposed a hybrid energy storage system integrating electrolyzers, fuel cells, and hydrogen storage components connected to solar PV, providing stable emergency power supply. This solution was proven effective in terms of cost and environmental impact, contributing to reduced greenhouse gas emissions and more sustainable energy use. Additionally, study¹⁶⁰ concerning a hybrid hydrogen/battery system for a grid-connected building showed a reduction in carbon emissions to 0.15 kg_{CO₂eq} kW⁻¹ h⁻¹, while a study on seasonal hydrogen storage in Finland demonstrated a 69% reduction in CO₂ emissions and decreased reliance on fossil fuels.¹⁶¹

Looking ahead, a hydrogen distribution network is projected to encompass 5000 km of pipelines by 2030,²³ marking a significant step toward large-scale hydrogen adoption.

Building on the current state of research, the present paper aims to contribute to the scientific field by presenting a numerical tool designed for energy and environmental analysis of H2PEM power stations, which are expected to play an increasingly prominent role in the energy systems of the near future.

H2PEM system layout

After a thorough review of the literature, the focus shifts to the core of the work. The embodiment of this system, herein referred to as the H2PEM system or power station, is illustrated in Fig. 3.

It can be interfaced with a power network, integrating with other energy systems to either deliver energy services to specific users or help maintain the electrical balance through the management of energy inflows and outflows. The H2PEM system consists of the key components: a PEMEL Electrolysis unit for hydrogen production, a PEMFC fuel cell unit for generating electricity, and a dedicated hydrogen storage unit that incorporates both hydride (MHD) and compression (H2C) methods for enhanced storage capacity and system flexibility.

Additionally, DC/DC converters serve to stabilizing voltage amidst the fluctuating energy transfers. An external power supply is necessary when additional energy is needed from the centralized network to produce hydrogen.

The PEMEL electrolysis unit is supported by several auxiliary components, including a demineralized water reservoir and temperature regulation systems, which ensure optimal heat management and operational efficiency. Additionally, a conditioning power system facilitates interaction with the external environment. The PEMEL functions as a hydrogen generator under an applied electrical stimulus, maintained at a constant

[¶] <http://www.haeolus.eu/>.



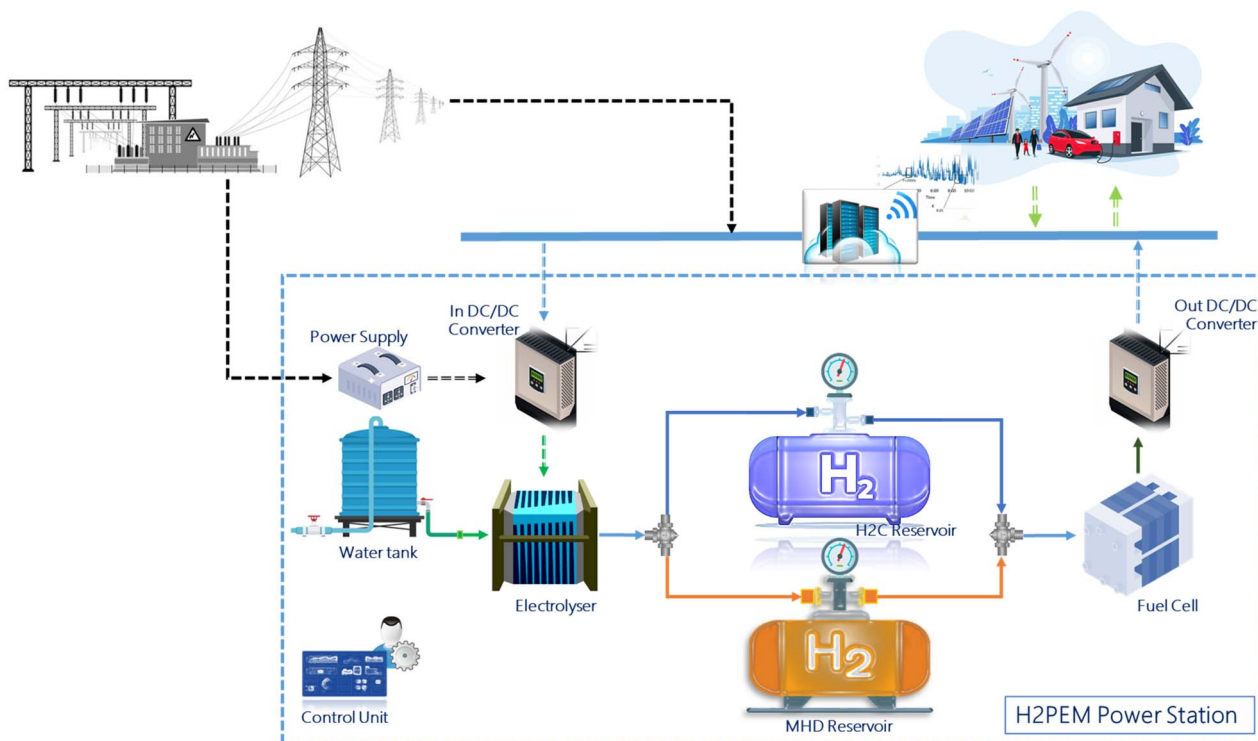


Fig. 3 H2PEM energy system layout.

voltage. Consequently, the 'in' DC/DC power converter adjusts the voltage–current pair required for the electrolyzer's proper operation.

Similarly, the PEMFC fuel cell unit includes a process air supply system, as well as auxiliary subsystems for operational management. However, a dedicated section provides a detailed analysis of the balance of plant for each individual unit. The 'out' DC/DC converter, as mentioned previously, is responsible for delivering voltage-controlled electrical power.

The decision to employ two different hydrogen storage technologies in this work is directly informed by the literature study presented earlier. As discussed, conventional compression storage has limitations regarding storage capacity and mechanical stresses due to the cyclic charging–discharging process. In contrast, metal hydride (MHD) technology offers significantly higher storage potential than compression systems. However, both technologies are adopted for several reasons. Firstly, having two storage systems increases the resilience of the entire system. If one is unavailable, the other can still provide support. Secondly, the MHD system requires much less space for storing the same amount of hydrogen. Thirdly, to reduce volume requirements, hydrogen in the H2C must be highly pressurized. This necessitates the use of a hydrogen compressor, which can lower overall system efficiency. The compressor requires energy to operate, which, in a self-sustaining system, would ideally be supplied by the fuel cell using hydrogen from the MHD. In extreme cases, the system could rely on external grid energy. Finally, the option of using very low pressure for hydrogen storage is possible, and in this

case, storage can be effectively managed by utilizing the pressure from the electrolyzer.

As noted in the literature, commercial PEM electrolyzers can efficiently produce hydrogen at pressures up to 15–30 bar. In the case of hydrogen usage in PEM fuel cells (PEMFC), this would necessitate a pressure reducer that does not impose extreme pressure reductions. Commercial PEMFCs typically operate within a pressure range of 6 to 20 bar.

This work introduces a standardized methodology that can be replicated and extended for different applications. As emphasized throughout, one of the main advantages of both fuel cells and electrolyzers is their modularity. By stacking cells in series, voltage requirements can be met, while parallel arrangements adjust the current requirements. Therefore, modules are coupled in parallel to meet the user's power delivery needs, allowing the system to scale easily. As mentioned in previous sections, literature suggests system sizes ranging from a few kilowatts to megawatts. However, the focus of this work is on smaller-scale systems, specifically around 1 kW of nominal electric power for both the electrolyzer and fuel cell.

Consequently, the hydrogen storage system also needs to be appropriately sized. The logic applied here is to ensure a storage capacity that can cover at least one full day in the event of a total blackout of the external electrical network. This would enable the fuel cell to provide energy for a sufficient number of hours to restore the network. The design of the system, coupled with the control strategy developed in this work, helps to optimize costs by streamlining the management of incoming and outgoing





Table 2 Steady state modeling for PEMFC and PEMEL

	Fuel cell (PEMFC)	Electrolyzer (PEMEL)
Energy conservation	$P_{in} - P_{out} = C_t \cdot \frac{dT}{dt}$ (1)	
Mass conservation	$\dot{m}_{in} - \dot{m}_{out} = \frac{dm}{dt}$ (2)	
Electrochemical reaction	$H_2 \rightarrow 2H^+ + 2e^-$ anode $\frac{1}{2}O_2 + 2H^+ + 2e^- \rightarrow H_2O$ cathode (3fc)	$H_2O \rightarrow \frac{1}{2}O_2 + 2H^+ + 2e^-$ cathode $2H^+ + 2e^- \rightarrow H_2$ anode (3el)
Electric equations for stacks	$H_2 + \frac{1}{2}O_2 \rightarrow H_2O$ global $V_c^{fc} = E_{N_fc} - A \cdot \ln\left(\frac{j^{fc} + j_n}{j_0}\right) - (j^{fc} + j_n) \cdot ASR + B \cdot \ln\left(1 - \frac{j^{fc} + j_n}{j_L}\right)$ (4fc) $E_{N_fc} = -\frac{\Delta G_{fc}^0(T, p_0)}{n_e \cdot Fa} - \frac{\Re \cdot T}{n_e \cdot Fa} \cdot \ln\left(\frac{p_{H_2O}}{p_{H_2} \cdot p_{O_2}^{1/2}}\right) j^{fc} = j^{fc} \cdot A_{c,fc}$ (4el)	$H_2O \rightarrow H_2 + \frac{1}{2}O_2$ global $E_{N_el} = \frac{\Delta G_{el}^0(T, p_0)}{n_e \cdot Fa} + \frac{\Re \cdot T}{n_e \cdot Fa}$ $\ln\left(\frac{p_{H_2} \cdot p_{O_2}^{1/2}}{p_{H_2O}}\right) V_c^{el} = E_{N_el} + \frac{\Re \cdot T}{n_e \cdot \alpha \cdot Fa} \cdot \operatorname{arcsinh}\left(\frac{j^{el}}{j_0}\right)$ $+ R_{eq}(T) \cdot j^{el} j^{el} = j^{el} \cdot A_{c,el}$ (4el) $\dot{V}_{cat}^{out} = 1.348 \times 10^3 \cdot \frac{j^{el} \cdot n_c \cdot (\lambda_{el} - 1)}{2 \cdot n_e \cdot Fa}$ $\dot{V}_{an}^{out} = \dot{V}_{H_2}^{(p)} = 1.348 \times 10^3 \cdot \frac{j^{el} \cdot n_c}{n_e \cdot Fa}$ $\dot{V}_{O_2}^{(p)} = 1.348 \times 10^3 \cdot \frac{j^{el} \cdot n_c}{2 \cdot n_e \cdot Fa}$ $\dot{V}_{H_2O}^{(in)} = 1.348 \times 10^3 \cdot \frac{\lambda_{el} \cdot j^{el} \cdot n_c}{n_e \cdot Fa}$ $\dot{V}_{H_2O}^{(r)} = 1.348 \times 10^3 \cdot \frac{j^{el} \cdot n_c}{n_e \cdot Fa}$ $\dot{V}_{H_2}^{(p)} = 1.348 \times 10^3 \cdot \frac{j^{el} \cdot n_c}{n_e \cdot Fa}$ $\lambda_{el} = \frac{\dot{V}_{H_2O}^{(in)}}{\dot{V}_{H_2O}^{(r)}} (5el)$
Volumetric flow rates	$\dot{V}_{an}^{out} = 1.348 \times 10^3 \cdot \frac{j^{fc} \cdot n_c \cdot (\lambda_{H_2,fc} - 1)}{n_e \cdot Fa}$ $\dot{V}_{cat}^{out} = 1.348 \times 10^3 \cdot \frac{j^{fc} \cdot n_c \cdot (4.76 \cdot \lambda_{O_2,fc} + 1)}{2 \cdot n_e \cdot Fa}$ $\dot{V}_{H_2}^{(r)} = 1.348 \times 10^3 \cdot \frac{j^{fc} \cdot n_c}{n_e \cdot Fa}$ $\dot{V}_{O_2}^{(r)} = 1.348 \times 10^3 \cdot \frac{j^{fc} \cdot n_c}{2 \cdot n_e \cdot Fa}$ $\dot{V}_{H_2O}^{(p)} = 1.348 \times 10^3 \cdot \frac{j^{fc} \cdot n_c}{n_e \cdot Fa}$ $\dot{V}_{H_2}^{(in)} = 1.348 \times 10^3 \cdot \frac{\lambda_{H_2,fc} \cdot j^{fc} \cdot n_c}{n_e \cdot Fa}$ $\dot{V}_{air}^{in} = 6.4165 \times 10^3 \cdot \frac{j^{fc} \cdot n_c \cdot \lambda_{O_2,fc}}{2 \cdot n_e \cdot Fa}$ $\lambda_{H_2,fc} = \frac{\dot{V}_{H_2}^{(in)}}{\dot{V}_{H_2}^{(r)}}$ $\lambda_{O_2,fc} = \frac{0.21 \cdot \dot{V}_{air}^{in}}{\dot{V}_{O_2}^{(r)}} (5fc)$	

energy flows and minimizing the cost contributions associated with the use of a compressor for hydrogen pressurization.

Regarding the functioning modalities, the H2PEM activates to address imbalances in the electric grid, whether there is excess power (scenario a) or a deficiency (scenario b). In scenario (a), surplus electricity is converted into hydrogen for storage. In contrast, scenario (b) sees the power station converting stored hydrogen back into electrical energy to satisfy demand.

Numerical modeling

This section includes the comprehensive modeling of the H2PEM system. The exposition delves into the 0D steady-state modeling of individual subsystems, being the purpose of this work to analyze at system level.

Steady state modeling

Table 2 reports the modeling concerning PEMFC and PEMEL units. The equations employed span from eqn (1) to (5fc/el), where the subscript 'fc' signifies the fuel cell context, while 'el' pertains to the electrolysis system. The suite of equations encompasses the energy conservation eqn (1), the mass conservation eqn (2), the electrochemical reactions eqn (3fc) and (3el), the electric equation concerning the stacks of the electrochemical units eqn (4fc) and (4el), and the volumetric flow rates eqn (5fc) and (5el) of the fluids involved in the processes. The energy conservation eqn (1) is crucial for managing the thermal regulation of both the fuel cell and electrolyzer. These devices are designed to operate at low temperatures, making the proper management of energy flows essential to maintain the system's operating temperature. This aspect is further detailed in the energy analysis section. The mass balance eqn (2) is used to calculate the required flow rates, as outlined in eqn (5fc/el).

Eqn (3fc) and (3el) describe the reaction paths across the sandwich structure of anode–electrolyte–cathode for both the fuel cell and electrolyzer. For the fuel cell eqn (3fc), the anode is where hydrogen decomposes into protons (2H^+) and electrons (2e^-). The protons pass through the selective electrolyte to the cathode, while the electrons travel through an external circuit to reach the cathode. At the cathode, protons and electrons combine with oxygen to form liquid water. The overall reaction thus involves hydrogen and oxygen to generate electrical power and produce liquid water.

For the electrolysis process, the reaction follows the reverse path. Liquid water splits at the cathode into hydrogen protons and electrons, releasing half a molecule of oxygen. The hydrogen protons then combine with external electrons to form a hydrogen molecule.

The fuel cell process is spontaneous, generating electrical power, whereas the electrolysis process is non-spontaneous and requires an external power supply to proceed.

The equations, reported in eqn (4fc) and (4el), determine the key electrical parameters, primarily the voltage at the stack level as a function of the electric current. In the case of the fuel cell

(V_c^{fc}), the voltage equations account for polarization losses, while for the electrolyzer (V_c^{el}), they reflect the overvoltage.

The Nernst voltage ($E_{\text{N_fc}}$, $E_{\text{N_el}}$) represents the ideal voltage of the process, which is influenced by polarization phenomena (activation, ohmic, and concentration types). The electric current (i^{fc}) and (i^{el}) are typically determined as the product of the current density (j) and the reaction area (A).

Eqn (5fc) and (5el) calculate the flow rates within the subsystems as a direct function of the electric current, with units expressed in Nl min^{-1} . For example, for the fuel cell, the required hydrogen flow rate ($V_{\text{H}_2}^{(\text{in})}$) can be determined as a function of the desired electric current (i^{fc}), the number of cells in the stack (n_c), and other thermo-electrochemical parameters, such as the Faraday constant (F_a), the number of electrons exchanged (n_e), and the hydrogen excess factor ($\lambda_{\text{H}_2,\text{fc}}$). Similarly, the rest of the volumetric flow rates can be calculated using a comparable structure. The same approach applies to the electrolysis process. For more detailed information, refer to the Symbolology section.

These models follow established methodologies for PEMFC and PEMEL as documented in the literature. This foundational modeling will support the subsequent energy analysis, detailed in the following section, by calculating the net electric power output of the fuel cell unit and the power consumption of the electrolysis unit.

Dynamic modeling

The dynamic modeling is based on the electric double layer (EDL) phenomenon, which involves the accumulation of charges, including both electrons and protons, at the boundary between the cell's electrode and the electrolyte. The charge double-layer phenomenon is related to the characteristics of the equivalent capacitor, as described in expression (6).

$$C = \frac{Q}{E} = \epsilon_0 \cdot \frac{s}{d} \quad (6)$$

Consequently, when there is a sudden change in current, the activation overvoltage at both electrode sites is delayed in following the current shift due to the reaction kinetics. This phenomenon has a significant impact on electrochemical devices, including fuel cells and electrolyzers.^{162–166} Study¹⁶⁷ emphasized the consequences of neglecting the charge-double layer effect, revealing that rapid changes in input current can result in discrepancies exceeding 15% between static models and experimental data, particularly during transient operations. In contrast, the dynamic model showed an error rate of less than 4% compared to the experimental results.

This accumulation creates a capacitive effect at these boundaries.^{168–171} To effectively model this dynamic behavior, two RC branches are used to represent the EDL.

The dynamic interactions within the PEMEL and PEMFC subsystems are therefore represented by eqn (7) and (8), accordingly.



$$E_{id} - R_{an} \cdot \left(i - C \cdot \frac{dV_{an}}{dt} \right) - R_{mem} \cdot i - R_{cat} \cdot \left(i - C \cdot \frac{dV_{cat}}{dt} \right) - V_{real} = 0 \quad (7)$$

$$V_{real} - R_{an} \cdot \left(i - C \cdot \frac{dV_{an}}{dt} \right) - R_{mem} \cdot i - V_{int} - R_{cat} \cdot \left(i - C \cdot \frac{dV_{cat}}{dt} \right) = 0 \quad (8)$$

The reported values for double-layer capacitance are consistent with those commonly observed in supercapacitors, ranging from 3 to 69 F.¹⁷² In this study, the Larminie–Dicks model is utilized due to its established accuracy and practical applicability.¹⁷⁰ Fig. 4 presents the schematic representation of the electric equivalent approach.

The next step in this methodology involves identifying model parameters through a systematic comparative assessment with carefully selected literature data, which have been derived from experimental findings.

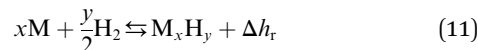
H₂ storage modeling

The initial phase involves modeling the compression tank sub-unit, whereby the state equation of the gas is applied. The relationship between pressure and the accumulated hydrogen mass within the tank is depicted by eqn (9), which takes into consideration the influence of real gas behavior through the van der Waals equation, parameterized by 'z'. Eqn (10) characterizes the temporal stored energy.

$$\frac{dp_{H_2C}(t)}{dt} \cdot V_{H_2C} = \frac{dm_{H_2}(t)}{dt} \cdot z \cdot \frac{\Re}{MW_{H_2}} \cdot T \quad (9)$$

$$E_{H_2}^{s,H_2C}(t) = z \cdot \frac{p_{H_2C}(t) \cdot V_{H_2C}}{\Re \cdot T_{H_2C}} \cdot LHV_{H_2} \quad (10)$$

Metal hydrides (MH) are distinguished by a reversible reaction (11) involving hydrogen and a metal alloy, encapsulating the heat of the reaction as denoted by Δh_r .



Some assumptions are adopted to streamline the model. These include: (1) the utilization of the ideal gas equation of state, (2) the consideration of negligible effects from compression work and viscous dissipation, (3) the assumption of negligible influence from radiative heat transfer, and (4) the premise of local thermal equilibrium with both gas and solid maintaining the same temperature.^{173–176}

The modeling framework is devoted to establishing a correlation between the tank's pressure, hydrogen concentration within the solid material, and the operational temperature eqn (12)–(17). Building upon the methodology introduced in the work by,¹⁷⁷ the present investigation undertakes the modeling of the metal hydride tank utilizing the Lacher modeling approach.^{178–180}

Eqn (12) calculates pressure as a composite of equilibrium pressure (p_{eq}) and the Lacher function. The equilibrium pressure is determined by Van't Hoff's eqn (13), which correlates the temperature (T) of the hydride with the reaction enthalpy (Δh_r) and entropy (Δs_r). The constancy of enthalpy and entropy changes can be assumed for a given material under a common reference point.^{181–183} Eqn (14) encapsulates the Lacher component of the model, contingent on the T/T_c ratio, which embeds insights into hydrogen absorption and desorption through the term represented by θ . Here, T and T_c correspond to the operating and critical temperatures of the metal hydride. The θ ratio eqn (15) delineates the proportion between H₂ concentration eqn (16) at time t and the hydride's maximum capacity. $E_{H_2}^{s,MHD}(t)$ signifies the H₂ energy stored at time t eqn (17).

$$\ln(p_{MHD}) = \ln(p_{eq}) + La^* \quad (12)$$

$$\ln(p_{eq}) = \frac{\Delta h_{r,MHD}}{\Re \cdot T_{MHD}} - \frac{\Delta s_{r,MHD}}{\Re} \quad (13)$$

$$La^* = \left\{ \left[\alpha_1 \cdot \frac{\ln(\theta)}{1 - \theta} \right] + \left[\alpha_2 \cdot \frac{T_{MHD}}{T_c} \cdot \left(\frac{1}{2} - \theta \right) \right] \right\} \quad (14)$$

$$\theta = \frac{c(t)}{c_{max}} \quad (15)$$

$$c(t) = \frac{m_{H_2,MHD}(t)}{m_{H_2,MHD}^{max}} \quad (16)$$

$$E_{H_2}^{s,MHD}(t) = \theta \cdot c_{max} \cdot m_{MHD} \cdot LHV_{H_2} \quad (17)$$

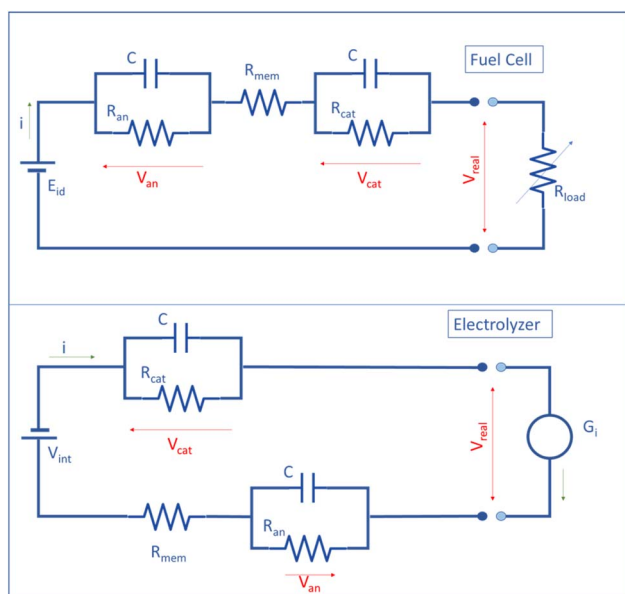


Fig. 4 H₂PEM equivalent circuit: fuel cell PEMFC and electrolyzer PEMEL.



Finally, $SOC(t)$ represent the state of charge of the storage unit, reported in eqn (18).

$$SOC(t) = \frac{E_{H_2}^s(t)}{E_{H_2}^{\max}} \quad (18)$$

Energy analysis

The energy analysis consists of assessing the energy-related parameters for machine energy-mappings. Therefore, it is necessary to know the energy involvement in fuel cell and electrolysis units. To this purpose Fig. 5 serves as showing the schematic representations of the Balance of Plant (BoP) configurations for both the units. The fuel cell unit delivers an electrical power, which is the gross quota of the stack, reduced by that required for the auxiliary components. Analogously for the electrolysis unit, its gross power constitutes the sum of the electric power essential for the stack, augmented by the contributions from auxiliaries. The BoP framework encompasses a comprehensive ensemble of elements, including blowers for air supply, blowers dedicated to cooling to effectively dissipate excess heat, electric warmers designed to heat-up in case of over-cooling, and electric warmers tasked with heating the fluids entering the devices. DC/DC converters serve to electric power conveyance.

Table 3 presents the key eqn (19)–(26) used for conducting the energy analysis. Eqn (19fc) and (19el) calculate the stack electric power, which is essential for extending the energy analysis to the entire system. In this context, this is depending on the number of the cells that constitute the fuel cell or the electrolyzer. Additionally, if the system exceeds the thermoneutral condition, the subsystems generate heat. This is caused by side reactions involving overpotentials. Fuel cell easily operate above the thermoneutral point, as governed by spontaneous and exothermic processes. In electrolyzers, when operating beyond the thermoneutral point, additional energy (usually in the form of increased voltage) is needed to drive the

water electrolysis reaction. This extra energy, which is not used to split water molecules, manifests as excess heat. This excess heat is described by eqn (20fc) and (20el). Consequently, this heat must be dissipated to prevent overheating of the device. Analyzing the equations, these mainly depends on the reaction enthalpy, the voltage and electric current operated.

Eqn (21)–(24) detail the auxiliary power requirements necessary for system operation, based on the schematic in Fig. 5. Eqn (21) indicate the required electric power for air venting, necessary to cool the fuel cell or the electrolyzer. Eqn (22) determines the power to blow air to cathode of the fuel cell. Eqn (23) regards the electric power employed to warm the fluids and prepare them. Eqn (24) calculates the electric power to heat the device. As a consequence, the electric power at the terminals of both the fuel cell and electrolysis units is determined using eqn (25fc) and (25el), accounting for all auxiliary power needs for system self-sustenance. The electric power of the fuel cell, as a net contribution delivered to the terminals ($P_{DC/DC}^{(net,out)}$), is given by the stack power, which is the gross quota, diminished of the electric power required for each auxiliary component.

Conversely, the electric power required to operate the electrolyzer is determined by the gross power ($P_{DC/DC}^{(gross,in)}$), which accounts for the electrical power needed by the stack for the electrochemical process, in addition to all auxiliary power contributions.

Finally, the efficiencies are calculated using eqn (26fc) and (26el). For the fuel cell, the efficiency is the ratio between the net electrical power at the terminals and the chemical power provided by the hydrogen fed into the system. For the electrolyzer, the conversion efficiency is the ratio of the chemical power in the hydrogen produced to the total electrical power supplied to the system. These equations are expressed as functions of primary parameters, such as reaction enthalpy variation, electric current, and auxiliary power contributions.

To the scope of determining the ventilation requirements for cooling both the fuel cell and the electrolyzer, standard aeraulic expressions are used. For fuel cells this is calculated from the

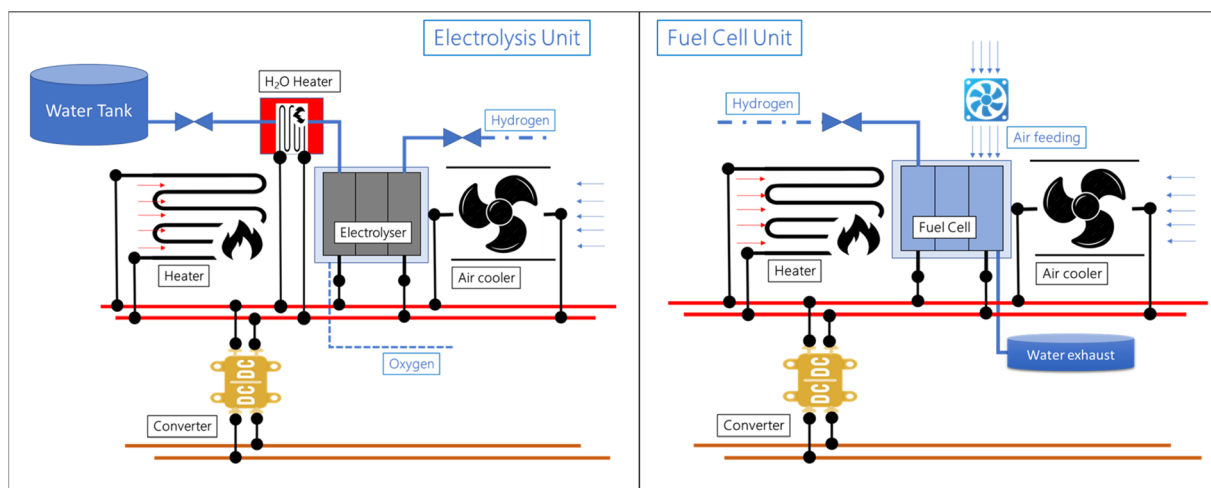


Fig. 5 Balance of Plant for electrolysis unit and fuel cell unit.



Table 3 Energy analysis

	Fuel cell (PEMFC)	Electrolyzer (PEMEL)
Electric power of the stack	$P_{\text{el}}^{(p)} = n_c \cdot V_c^{fc} \cdot i^{fc} \quad (19\text{fc})$	$P_{\text{el}}^{(in)} = n_c \cdot V_c^{el} \cdot i^{el} \quad (19\text{el})$
Thermal equations	$P_{\text{th}}^{(p)} = -\frac{n_c \cdot i^{fc}}{n_e \cdot Fa} [\Delta \tilde{h}_{r,H_2} + (n_e \cdot Fa \cdot V_c^{fc})] \quad (20\text{fc})$	$P_{\text{th}}^{(\text{gen})} = -\frac{n_c \cdot i^{el}}{n_e \cdot Fa} [\Delta \tilde{h}_{r,H_2O} - (n_e \cdot Fa \cdot V_c^{el})] \quad (20\text{el})$
Blower power for air cooling	$P_{\text{blow}}^{\text{cool}} = \frac{\dot{V}_{\text{air}} \cdot \Delta p_{\text{tot}}}{\eta_{\text{blow}}} \quad (21)$	
Blower power for air supply	$P_{\text{blow}}^{\text{air,in}} = \frac{\dot{V}_{\text{air}} \cdot \Delta p_{\text{tot}}}{\eta_{\text{blow}}} \quad (22\text{fc})$	
Electric power for fluid warming	$P_{\text{fluid}}^{\text{warm}} = \frac{F_{\text{fluid}}^{\text{in}} \cdot \Delta \tilde{h}_{\text{fluid}}^{\text{in}}}{\eta_{\text{el}}} \quad (23)$	
Electric power for device warming	$P_{\text{fc/el}}^{(\text{el-warm})} = \frac{m_{\text{fc/el}} \cdot c_p \cdot \Delta T}{\eta_{\text{el}}^{\text{warm}}} \quad (24)$	
Electric power at system terminals	$P_{\text{FC}}^{\text{stack(gross)}} = P_{\text{el}}^{(p)} = P_{\text{DC/DC}}^{(\text{net,out})} + \Delta P_{\text{DC/DC}}^{(\text{out})} + P_{\text{AIR}}^{(\text{sup})} + P_{\text{AIR}}^{(\text{cool})} + P_{\text{fc}}^{(\text{el-warm})} + P_{\text{in-gas}}^{(\text{warm})} \quad (25\text{fc})$	$P_{\text{EL}}^{\text{stack(net)}} = P_{\text{el}}^{(\text{us})} = P_{\text{DC/DC}}^{(\text{gross,in})} - \Delta P_{\text{DC/DC}}^{(\text{in})} - P_{\text{AIR}}^{(\text{cool})} - P_{\text{H}_2\text{O}}^{(\text{warm})} - P_{\text{el}}^{(\text{el-warm})} \quad (25\text{el})$
Efficiency	$\eta_{\text{el}}^{fc} = \frac{n_c \cdot i^{fc} \cdot V_c^{fc} - P_{\text{el}}^{(\text{aux})}}{i^{fc} \cdot n_c \cdot \Delta \tilde{h}_{r,H_2}} \quad (26\text{fc})$	$\eta_{\text{H}_2}^{el} = \frac{\frac{n_c \cdot i^{el}}{n_e \cdot Fa} \cdot \Delta \tilde{h}_{r,H_2O}}{n_c \cdot V_c^{el} \cdot i^{el} + (P_{\text{th}}^{(\text{el,in})} - P_{\text{th}}^{(\text{gen})}) + P_{\text{el}}^{(\text{aux})}} \quad (26\text{el})$

equation shown in eqn (27), while eqn (28) is used for the electrolyzer. The criterion approached is that of keeping the temperature constant at each work conditions. Any excess thermal power is carefully managed, either dissipated or integrated, depending on the current operating conditions. Heat is dissipated through air venting into the channels of the electrochemical devices. Conversely, in case of cooling, heat needs to be supplied. This provision is done by overheating the fluids.

As regards the heat dissipation process, it refers exclusively to heat exchange by forced convection through the cooling air flow. The radiative heat exchange is neglected.

$$F_{H_2}^{\text{in}} \cdot \Delta \tilde{h}_{H_2}^{\text{in}} + F_{\text{Air}}^{\text{in}} \cdot \Delta \tilde{h}_{\text{Air}}^{\text{in}} + [(V_{\text{tn}}^{\text{fc}} - V_{\text{st}}^{\text{fc}}) \cdot i^{fc}] + F_{\text{Air}}^{\text{in,cool}} \cdot \Delta \tilde{h}_{\text{Air}}^{\text{in,cool}} \\ = F_{H_2O}^{\text{out}} \cdot \Delta \tilde{h}_{H_2O}^{\text{out}} + F_{\text{Air}}^{\text{out}} \cdot \Delta \tilde{h}_{\text{Air}}^{\text{out}} + F_{\text{Air}}^{\text{out,cool}} \cdot \Delta \tilde{h}_{\text{Air}}^{\text{out,cool}} \quad (27)$$

$$F_{H_2O}^{\text{in}} \cdot \Delta \tilde{h}_{H_2O}^{\text{in}} + [(V_{\text{st}}^{\text{el}} - V_{\text{tn}}^{\text{el}}) \cdot i^{el}] + F_{\text{Air}}^{\text{in,cool}} \cdot \Delta \tilde{h}_{\text{Air}}^{\text{in,cool}} \\ = F_{H_2}^{\text{out}} \cdot \Delta \tilde{h}_{H_2}^{\text{out}} + F_{O_2}^{\text{out}} \cdot \Delta \tilde{h}_{O_2}^{\text{out}} + F_{\text{Air}}^{\text{out,cool}} \cdot \Delta \tilde{h}_{\text{Air}}^{\text{out,cool}} \quad (28)$$

Environmental analysis

The environmental analysis is based on determining the CO₂ “equivalent” emissions and the associated climate implications in terms of temperature change. CO₂ productions and emissions are computed with hydrogen production and its subsequent use in electricity generation. Three scenarios are considered.

(1) Electrolysis powered by grid electricity: the electrolysis unit operates using electricity from the conventional electricity grid. The emissions are estimated based on the average CO₂ intensity of the grid electricity, which includes totally fossil fuels (coal, natural gas, oil).

(2) Electrolysis powered by grid electricity, considering the current energy share: the electrolysis unit operates using

electricity considering the current energy share of the grid, as a combination of renewable sources (solar, wind, and hydro) and conventional energy sources. The CO₂ emissions are calculated by determining the emissions intensity of the electricity mix fed into the electrolysis unit. This analysis considers the proportion of renewable and conventional energy sources in the network and their respective CO₂ emission factors.

(3) Electrolysis powered by a renewable-dominated energy network: the electrolysis unit is powered by a higher-level energy network consisting totally of renewable sources.

The analysis is therefore structured into the following key components:

CO₂ emissions from electrolysis – first the CO₂ emissions associated with hydrogen production *via* electrolysis are calculated.

Impact on climate change – the climate change implications in this study are assessed by estimating the temperature increase due to CO₂ emissions. This involves Temperature Increase Modeling. This step utilizes data from climate science literature to link CO₂ emissions with potential changes in global temperatures.

CO₂ savings analysis – the CO₂ savings are computed by comparing the CO₂ emissions from H2PEM to those from conventional fossil fuel-based systems. The calculation includes:

- Emission savings during hydrogen production: the CO₂ emissions saved by producing hydrogen from a mix of renewable energy sources compared to using fossil fuel-based electricity. This is determined by calculating the difference in CO₂ emissions between the renewable-powered electrolysis and fossil fuel-powered electrolysis.

- Emission savings during electricity generation from hydrogen: this is conducted evaluating the CO₂ emissions avoided by using the hydrogen fuel cell to generate electricity instead of a conventional power plant.



The model for calculating CO₂ emissions and the associated temperature increase involves the following equations.¹⁸⁴ Eqn (29) estimates the CO₂ emissions per kilogram of hydrogen produced when the electrolysis unit is powered by electricity from the grid. Eqn (30) calculates the contribution of fossil fuels to CO₂ emissions per kilogram of hydrogen produced. Eqn (31) determines the CO₂ emissions per kilogram of hydrogen when the electrolysis unit is powered by a mix of renewable and conventional energy sources. Eqn (32) calculates the amount of fossil fuel required to generate the equivalent electrical power ($P_{\text{el}}^{\text{fc}}$) that would otherwise be produced by the fuel cell. This calculation is used to estimate the CO₂ emissions avoided by using the hydrogen fuel cell. Eqn (33) calculates the temperature increase resulting from the change in atmospheric CO₂ concentration (Δc [ppm]).^{185,186} The term 'S' is the continuous "climate sensitivity" parameter.¹⁸⁶ The estimation of global warming takes into account not only the increase in CO₂ concentrations but also the rising levels of other greenhouse gases. The uncertainty range is represented between $S = 2.0$ °C and $S = 3.1$ °C.

$$X_{\text{CO}_2}^{\text{grid}} = 1e - 3 \cdot m_{\text{f}}^{\text{s}} \cdot \text{LHV}_{\text{f}} \cdot e_{\text{f}}^{\text{fa}} \quad (29)$$

$$m_{\text{f}}^{\text{s}} = 3.6 \cdot \frac{1}{\eta_{\text{el}}^{\text{f}}} \cdot \frac{E_{\text{H}_2}^{\text{s}}}{\text{LHV}_{\text{f}}} \quad (30)$$

$$X_{\text{CO}_2}^{\text{comb}} = E_{\text{H}_2}^{\text{s}} \cdot [(C_{\text{s}} \cdot E_{\text{s}}) + (C_{\text{w}} \cdot E_{\text{w}}) + (C_{\text{h}} \cdot E_{\text{h}}) + (C_{\text{o}} \cdot E_{\text{o}})] \quad (31)$$

$$m_{\text{f}}^{\text{el,fc}} = \frac{1}{\eta_{\text{el}}^{\text{f}}} \cdot \frac{P_{\text{el}}^{\text{fc}}}{\text{LHV}_{\text{f}}} \quad (32)$$

$$\Delta T(c) = S \cdot \log_2 \left(\frac{c_0 + \Delta c}{c_0} \right) \quad (33)$$

For definitions and explanations of the symbols used, please refer to the Symbolology section.

Settings, model assumptions and flowchart

For this purpose, a 1 H₂PEM kW system is conceived, with a H₂ storage capacity of 5 Nm³.

As planned, the storage volume capacity is selected to ensure operation for an entire working day, even in the event of an outage of the external energy network. For the fuel cell unit, a commercial PEM-based model from Ballard is used as the reference. It comprises a stack formed by 47 cells. Each cell has an active area of 100 cm².^{187,188}

The standard operating conditions for the fuel cell are 80 °C and 6 bar. The electrolysis unit consists of a stack of 6 electrolytic cells, each with an active area of 56 cm², and operates at 80 °C and 16 bar. It is based on a well-characterized single electrolytic cell model.^{189,190} The details of the electrolysis unit assembly, along with other fuel cell specifications, are reported in a subsequent section.

The tool is primarily designed for low-capacity H₂PEM power systems (1–10 kW). Its balance of plant focuses on auxiliary components suitable for small-scale systems, particularly in terms of thermal management, while the hydrogen storage section is sized accordingly. In this work, thermal management is achieved using air. However, for larger systems, it is more appropriate to implement thermal management using a liquid-based system.¹⁹¹ As the system size increases, certain governing parameters may need to be updated or scaled up—such as improving auxiliary system efficiency, which typically enhances in larger systems, larger storage capacity, *etc.*¹⁹² These adjustments are straightforward. Specifically, when adapting the thermal management for a larger system, modifications would involve altering the energy balance, replacing the air-based thermal management system with a liquid-based one, and changing the mover from a blower to a pump. Furthermore, this work does not include an additional compressor for hydrogen pressurization prior to storage. Instead, the innovation lies in operating at low pressures, where the electrochemical compression of the electrolyzer is utilized. This approach leverages the capability of commercial electrolyzers, which are already capable of operating efficiently at pressures between 15 and 30 bar. Therefore, hydrogen is pressurized in the tanks directly *via* electrolyzer.

As anticipated, for this scope the use of metal hydrides for hydrogen storage becomes more significant, as their ability to accumulate large quantities of hydrogen at relatively low pressures is repeatedly emphasized as one of their key advantages. Ultimately, the H₂ storage unit consists of an H₂C tank with a capacity of 2 Nm³, and a MHD tank with a capacity of 3 Nm³. The rest of the setting parameters can be viewed in the Table 4.

The assumptions for simulations are listed below:

- 0D-detail modeling;
- PEMFC/PEMEL – heat evacuation is considered to take place exclusively *via* forced convection of the cooling air, thus

Table 4 Main parameters of model settings for simulations

Fuel cell energy unit (PEMFC)			
Number of cells	n_{c}	47	
Active area		100	cm ²
Catalyst – Pt			
Electrolysis unit (PEMEL)			
Active area		56	cm ²
Catalyst – Pt/Ir			
Number of cells	n_{c}	6	—
H₂ storage unit			
H₂C			
Volume storage	$V_{\text{H}_2\text{C}}$	2	Nm ³
Minimum pressure	p_{min}	6	bar
Maximum pressure	p_{max}	16	bar
MHD			
Volume storage	V_{MHD}	3	Nm ³
Minimum pressure	p_{min}	11	bar
Maximum pressure	p_{max}	16	bar



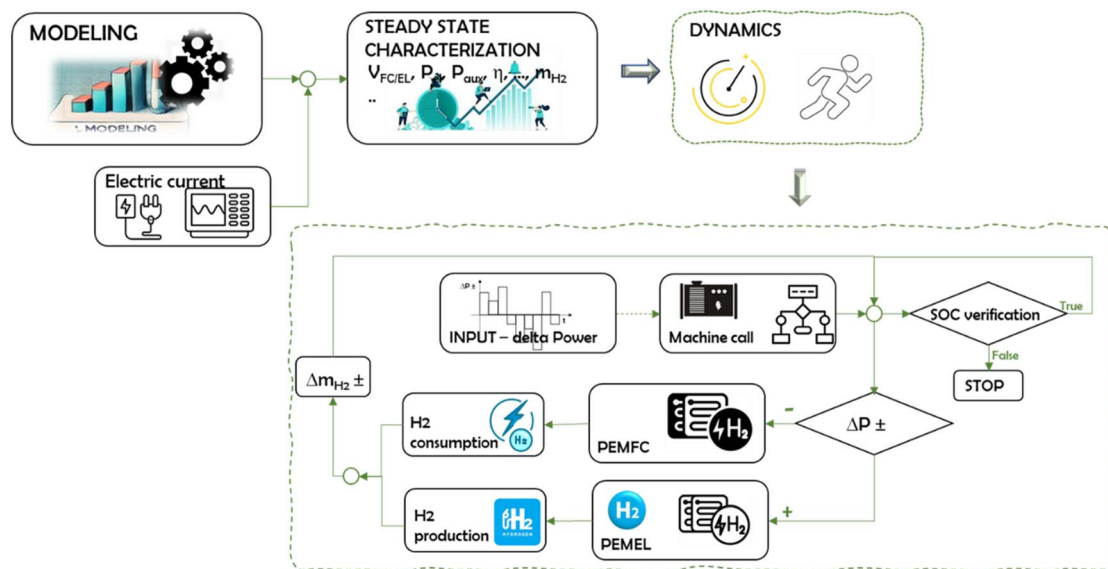


Fig. 6 Model flowchart.

neglecting the natural (non-forced) convective-radiative heat exchange with the external environment.

- PEMFC/PEMEL – isothermal process;
- PEMFC/PEMEL – cold start-up and shut-down stages not considered;
- PEMFC/PEMEL – fast electric response of auxiliary components;
- MHD – negligible effects from compression work and viscous dissipation;
- MHD – negligible influence from radiative heat transfer;
- MHD – local thermal equilibrium with both gas and solid maintaining the same temperature.
- MHD – isothermal process.

The model is codified, implemented and run in the Matlab/Simulink computational environment.

The integration of the single components needs to be managed by a superior control strategy, whose foundation is based on the model algorithm. Fig. 6 illustrates the flowchart that governs the logic behind the modeling algorithms. A streamlined representation of the algorithm's computational blocks is provided, minimizing diagram complexity to ensure that even less experienced users can easily follow the operational flows.

The modeling is based on the governing equations detailed in a previous section. The second step involves the steady-state characterization, serving as analyzing the system's energy behavior under various electric currents. This helps determine system performance metrics such as electric power, energy usage, conversion efficiencies, and hydrogen production or consumption. Once the system's performance is mapped, the dynamics block links the H2PEM system with a higher-level network that can operate both on-grid and off-grid. This dynamics block receives an input signal of positive or negative electric power.

This signal activates the system, directing it to the State of Charge (SOC) verification block. If the SOC exceeds its boundary

limits, the process halts; otherwise, the signal is routed to either the PEMFC (for $\Delta P-$) or the PEMEL (for $\Delta P+$). This routing results in hydrogen consumption or production, which adjusts the SOC. In this algorithm, priority is given to the Metal Hydride (MHD) reservoir, while the Compressed Hydrogen (H2C) reservoir serves as an emergency or backup system, activating only when the MHD SOC exceeds its limits.

The computational architecture of the H2PEM system utilizes a dynamic array to efficiently handle time-variant signals, leveraging arrays and matrices to optimize data processing. Decision-making is carried out through an “if-else/while/for” structure, with the “if-else” framework being essential for ON/OFF decisions regarding machine operations and directing computational signals. The “while” loop is particularly crucial for handling complex variables that require iterative techniques, such as determining the voltage-current coupling in the electrochemical stack. The model operates within a thermo-electrodynamics framework, continuously updated with key variables like enthalpies, flow rates, temperatures, and pressures. This ensures the system remains adaptable to varying external power conditions while accounting for system constraints and limitations in terms of response and capacity.

As deductible from Fig. 2, the primary goal is to characterize the H2PEM system from both an energy and environmental perspective.

Validation

The numerical modeling is validated for each component (fuel cell unit, electrolysis unit, and metal hydride storage) based on experimental data from the reference literature. Additionally, the H2PEM power station is dynamically validated as an integrated system, with comparisons made to experimental data. Details of the validation process can be found in the authors' prior study.¹⁹³



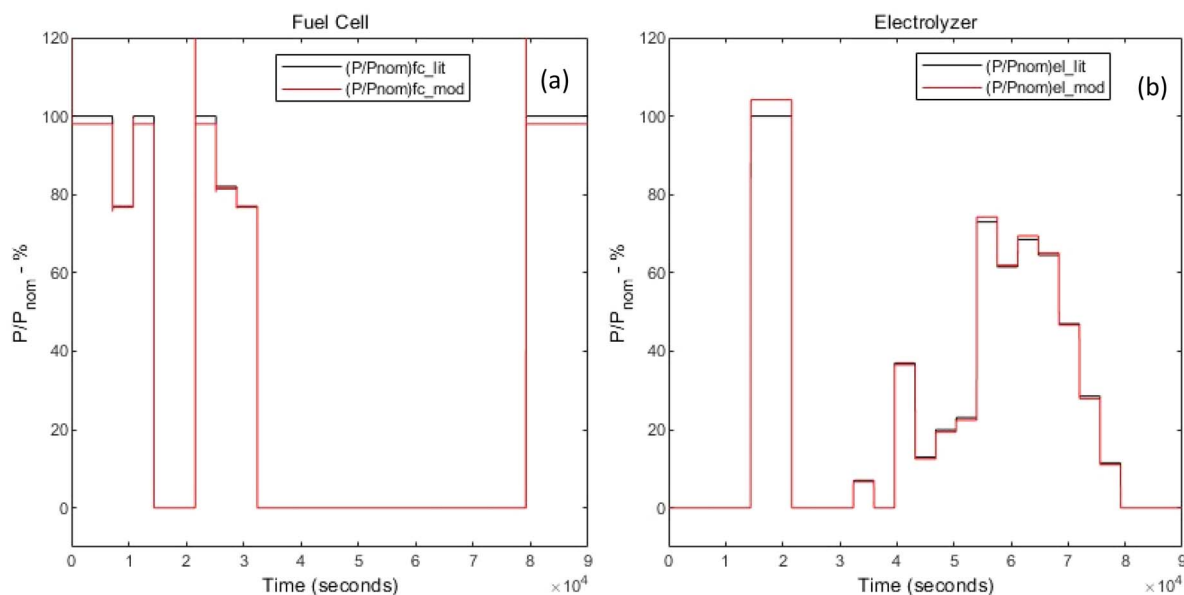


Fig. 7 System validation during fuel cell (a) and electrolyzer (b) call (black: literature, red: model).

Furthermore, an additional system model validation is performed with literature data¹⁹⁴ referring to a renewable energy network, containing among the sub-systems also an electrolysis unit and a fuel cell unit. The configuration and load requests are recreated in the Matlab/Simulink computational environment. The simulations are carried out in dynamic regime and are conducted over a 15-hour time window. Fig. 7 compares literature data and model results in terms of electric power exchanged inflow and outflow as a function of the time loads. Literature data and model results match for all the investigated conditions and parameters, indicating the accuracy of the present methodology.

Energy involvement in steady state regime

This section presents the energy analysis of the fuel cell and electrolyzer based on their operating pressures, as usually recommended by the manufacturers: 6 bar and 80 °C for the PEMFC, and at 16 bar and 80 °C PEMEL generates hydrogen. This first analysis is carried out at varying electric current. The analysis is then extended to include a broader range of possible operating temperatures and pressures.

Fuel cell

Fig. 8 illustrates the key stack and system performance parameters. In particular, the figure is organized into 4 graphs showing (a) the power curves with the auxiliary contributions, therefore the net system one, (b) the stack and system efficiency curve, (c) the hydrogen consumption profile, (d) the profile of the electrical ratio between the gross power and net system power. A detailed analysis of the auxiliaries' power consumption is provided at the end of this section.

Zooming into chart (a), the electrical power curve of the system, which reaches its maximum value of about 1376 W just over 50 A. The electric power curve associated to the auxiliaries has an increasing value with the current, with a profile that tends to assume an almost exponential trend at high currents, and this is mainly due to the high heat to be evacuated due to the aforementioned irreversibility. Taking into account the internal electrical self-absorption, the net power of the system assumes its maximum of about 1073 W at an electric current of 45.28 A. Therefore, about 250 W have to be destined to sustain the fuel cell as system. This self-sustainability is clearly reflected also in the electrical efficiency. Graph (b) illustrates the stack and system electrical efficiency profiles. The profiles have a trend similar to the polarization curve, therefore with a decreasing trend with the current. An offset increasing with current separates the stack efficiency profile from the system one. The stack efficiency assumes the value of 46% at the nominal current of 51.28 A, while the electrical system efficiency assumes the value of 40.5% at the nominal system current of 45.28 A. Graph (c) shows the trend of hydrogen consumption, which is quite linear, except in the vicinity of the streams where the polarization by concentration begins to have an influence. Clearly, it is worth underlining that the fuel cell is operated in the safety field, therefore long before the onset of concentration phenomena that are dangerous for operation. At nominal conditions the hydrogen consumption is higher than 12 Nl min^{-1} . Finally, the power ratio (chart (d)) between the stack electrical power and the net system electrical power reflects the influence of internal self-absorption. A power ratio close to 1.2 can be considered in the operating range of the fuel cell.

Electrolyzer

Fig. 9 shows the performance analyses for what concerns electrolysis system. It is based on a single cell (characterized in



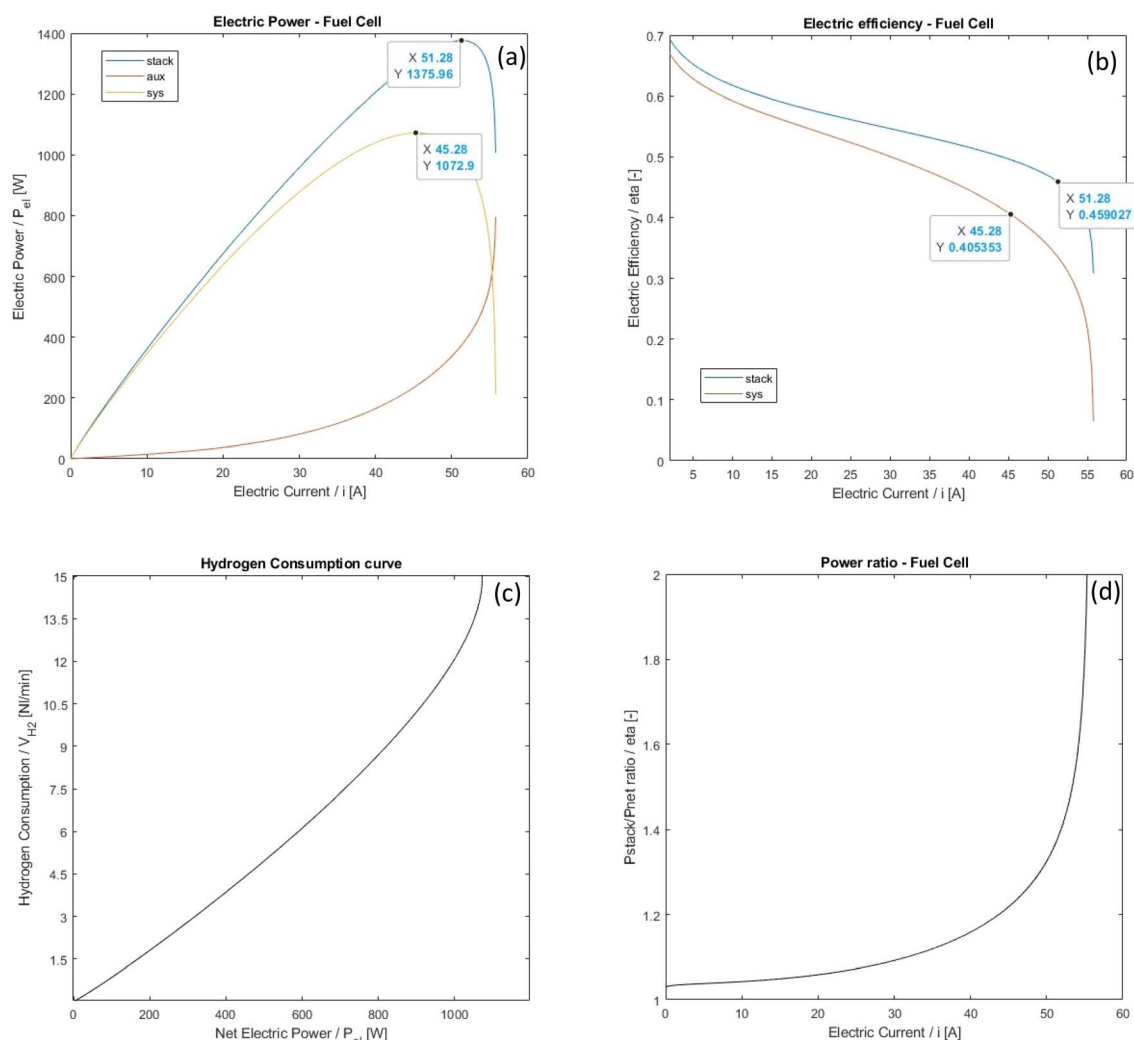


Fig. 8 Performance charts of the fuel cell unit: (a) electric powers, (b) electric efficiency, (c) hydrogen consumption, (d) power ratio.

laboratory) and is scaled up to 1 kW to for the purpose of this work. For this, 6 cell stacked in series are required. The figure is organized in 4 graphs showing: (a) the voltage and power curves, (b) the power curves with the auxiliary contributions, therefore the net system one, (c) the hydrogen production profile, (d) the system efficiency curve together with the profile of the electrical ratio between the gross power of system and the power required by the stack. A nominal hydrogen production of 3 Nl min^{-1} is estimated. From the voltage and electric power curve, a supply electrical current of around 73.6 A is calculated, which reflects a voltage of 11.35 V and an electrical power absorption of about 850 W at stack level. Considering the net internal self-absorption for the maintenance of the auxiliary components, the gross power to be allowed in absorption to the electrolysis system must be increased by approximately 160 W, bringing the power absorption to over 1 kW. This makes it possible to evaluate the electrolysis efficiency at the system level which assumes a parabolic-like profile with the current. The maximum electrolysis efficiency value is around 55%, for electric current values of 40 A. At maximum electric current, the

electrolysis efficiency decreases but remains at interesting values, around 50%.

Auxiliary components are essential for the system's functionality, as they are required for the operation of the PEMFC and PEMEL. However, they consume energy, which, as mentioned previously, needs to be supplied by the system itself for self-sustainability. In this context, the PEMFC and PEMEL are considered operational after their respective start-up phases, which are handled separately. For the PEMFC, auxiliary functions include air blowing for cooling and temperature regulation, air supply to the cathode, and heating fluids entering the system, such as hydrogen to the anode and air to the cathode. Since hydrogen is pressurized in the MHD and H₂C storage tanks, no dedicated mover is necessary for hydrogen transfer. For the PEMEL, auxiliary functions include water heating, ambient air blowing for cooling, and water pumping to ensure proper water flow into the electrolyzer to maintain its operation.

Fig. 10 presents the charts for the fuel cell unit, breaking down the power consumption into its key components. In chart



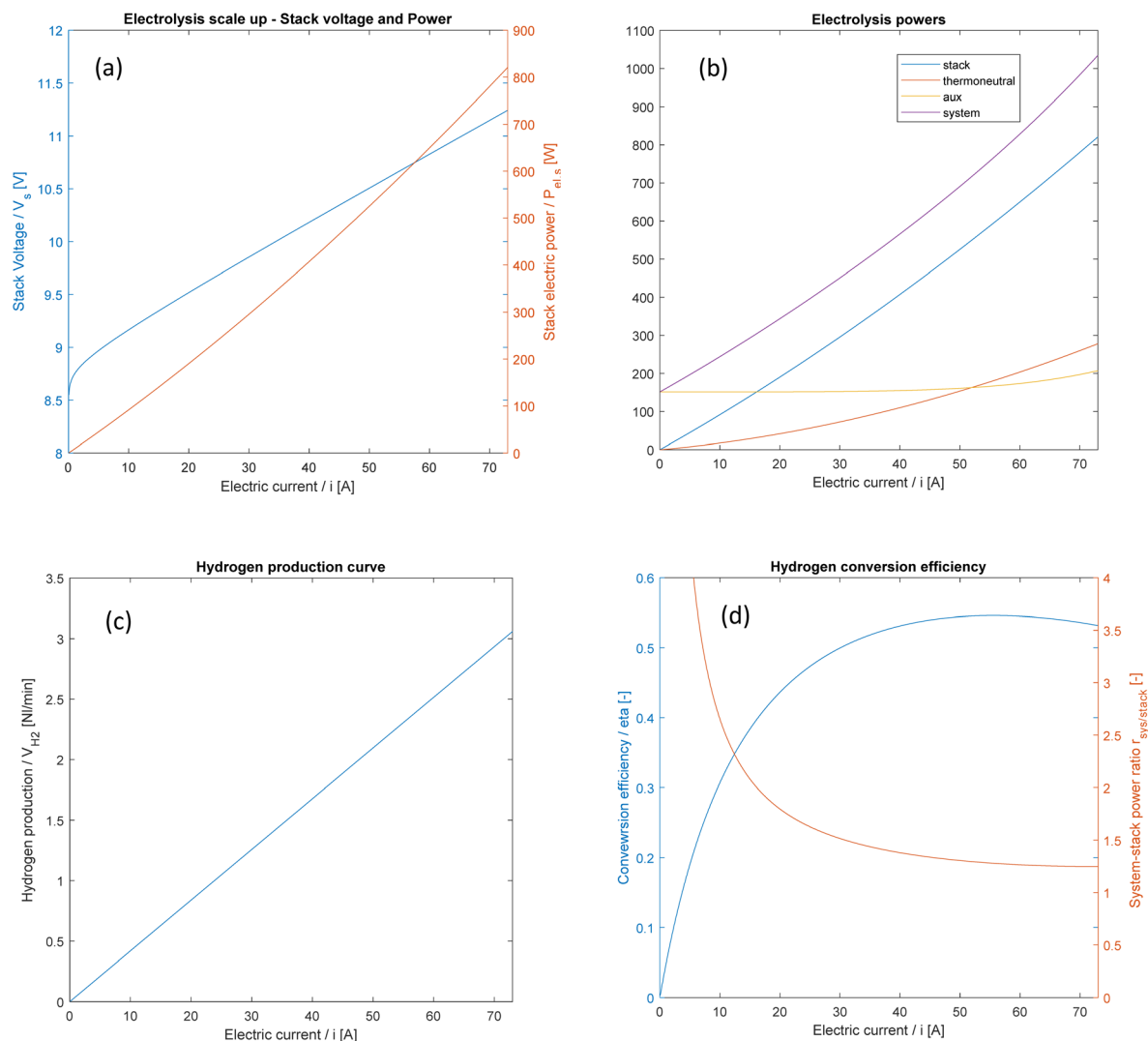


Fig. 9 Performance charts of the electrolysis unit: (a) stack voltage and electric power, (b) power contributions, (c) hydrogen production, (d) conversion efficiency and power ratio.

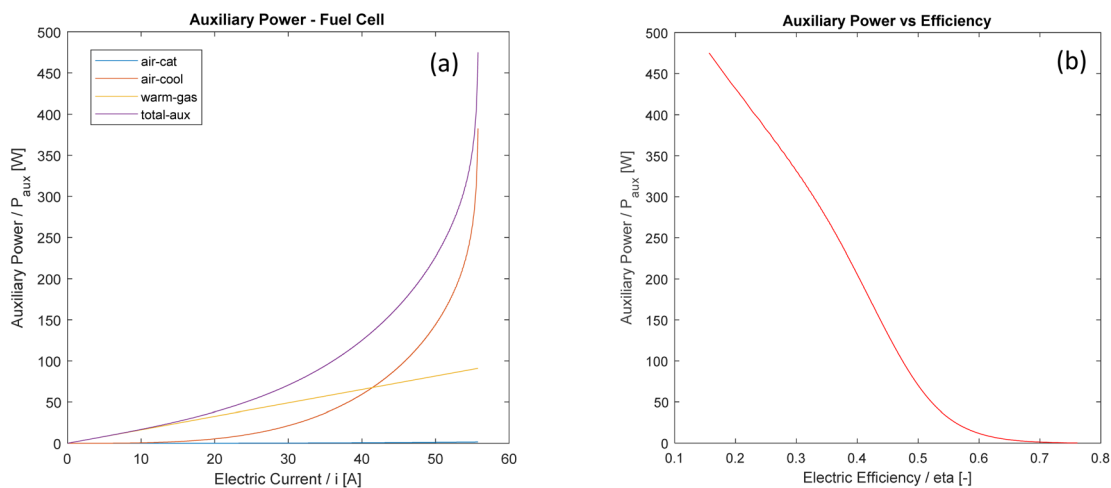


Fig. 10 Auxiliary analysis. Powers vs. electric current (a); power vs. electric efficiency (b).



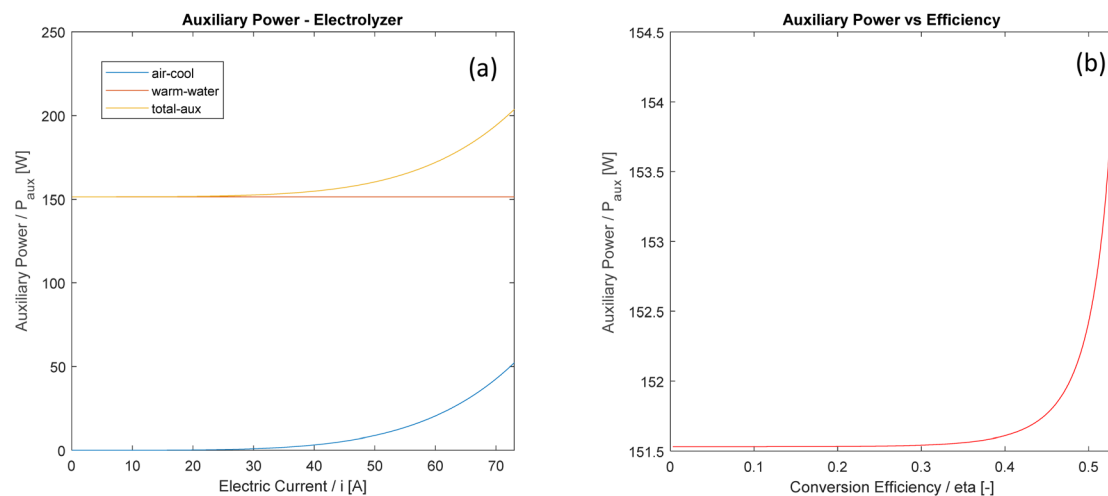


Fig. 11 Auxiliary analysis. Powers vs. electric current (a); power vs. conversion efficiency (b).

(a), it is evident that the power required to blow air into the cathode is negligible compared to the other contributions. The power needed to warm the reactant gases, on the other hand, follows a linear trend with the electric current, reflecting its direct proportionality – as the electric current increases, the demand for heated reactant fluids also increases. The most significant power consumption is associated with cooling, which uses ambient air. Once the fuel cell surpasses the thermoneutral condition and begins operating, the heat that must be evacuated shows an exponential trend, which becomes more pronounced as the system approaches its nominal operating conditions. At approximately 55 A, the auxiliary power required for safe fuel cell operation can exceed 450 W, potentially becoming the dominant contributor. Chart (b) assesses the

relationship between auxiliary power consumption and the system's electric efficiency. As expected, there is a direct correlation between the two. When auxiliary power consumption becomes more significant, the electric efficiency of the fuel cell declines, dropping to values as low as 20%.

Fig. 11 provides a similar analysis for the electrolysis unit. For the electrolyzer, a constant volume of water, approaching the maximum required amount, is continuously heated in preparation for use.

The heating power required for water typically hovers around 150 W. As the process progresses, air is introduced for cooling the PEMEL. Below 30–40 A, the cooling air power consumption is negligible, but it increases to approximately 50 W at the maximum operating current. As is well-known, electrolysis

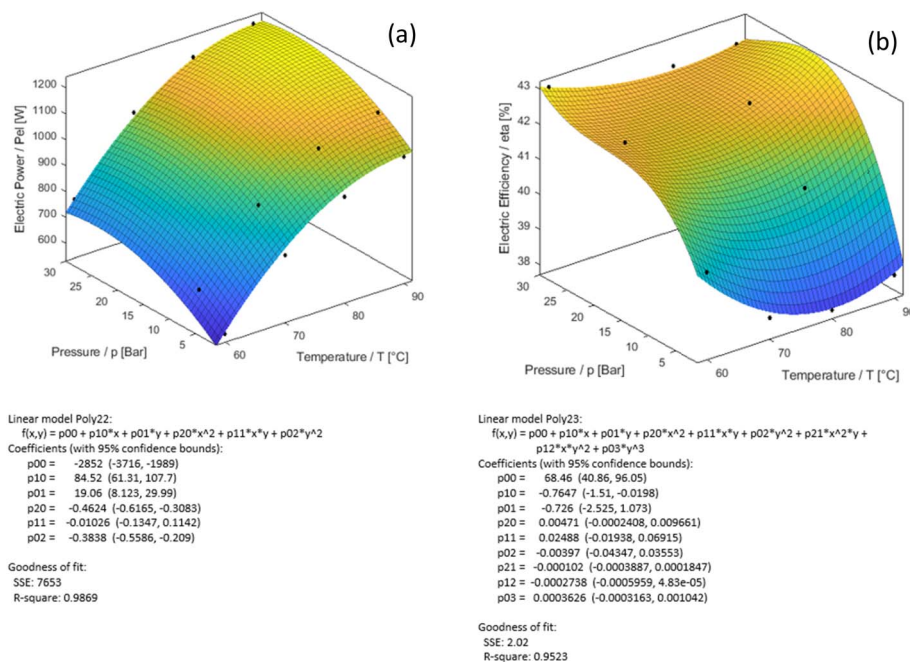


Fig. 12 PEMFC energy mapping. Net electric power delivered (a), net electric (system) efficiency (b).



requires both energy and heat to function. It is also important to note that the electrolyzer can generate excess heat if the thermoneutral condition is surpassed. To maintain temperature control, this excess heat must be evacuated, and the need for heat dissipation becomes more significant at higher currents, particularly above 40 A.

Discussion

Auxiliary power requirements are crucial factors that impact the efficiency of the system. This is especially true for smaller-scale systems, where precise control can be challenging. In this analysis, the subsystems are assessed from an energy perspective. As seen in the results, depending on the operational mode, the PEMFC unit shows a decreasing electric efficiency but an increasing electric power output, while the PEMEL unit exhibits increasing conversion efficiency and rising electric power consumption. In both cases, the auxiliary power consumption is the primary contributor to inefficiencies. A more comprehensive analysis, considering both technical and economic parameters, is necessary and should ideally be incorporated into an optimization framework.

Based on technical and operational constraints (e.g., PEMFC: highest power output or highest efficiency, with minimal associated costs; PEMEL: highest hydrogen production or highest conversion efficiency), the optimization solution will help determine the optimal operating conditions. Unfortunately, in the case of H₂PEM power station installations, their operation is often dictated by a higher-level energy network. The incoming and outgoing energy flows are determined by external signals. The control strategy plays a significant role in this: for example, configuring the H₂PEM system to always operate at nominal or maximum capacity optimizes the devices, minimizing capital expenditure and preventing oversizing.

Alternatively, the control strategy can be set to prioritize achieving the highest possible efficiency, in which case system oversizing should be considered to ensure efficiency is maximized despite increased capital costs.

Sensitivity analysis and performance mapping. This section presents the results focused on mapping the performance of both the PEM fuel cell and PEM electrolyzer. The analysis is complemented by a sensitivity study, which expands the operational parameters to include varying working pressures and temperatures. Specifically, a pressure range of 1–30 bar and a temperature range of 60–90 °C are considered. These operating conditions are within the feasible limits of the technologies.

The goal of these analyses is to identify the most advantageous operating conditions from an energy efficiency perspective and to generate a detailed performance mapping for both energy units. The electric power delivered by the fuel cell and absorbed by the electrolyzer, along with their respective energy conversion efficiencies, are carefully assessed. New 3D charts are introduced, with each chart accompanied by the corresponding 3D equations, derived using the Matlab fitting App. It is important to highlight that the kit of 3D equations can be useful for researchers and professionals, as it provides easily accessible data for application without the need for developing complex models or running computationally intensive simulations.

Fig. 12 illustrates the performance mapping for the fuel cell unit. Chart (a) shows the net electric power delivered, while chart (b) represents the electric efficiency at the system level. It can be observed that power increases with both temperature and pressure. As expected, temperature positively influences ohmic polarization, and pressure enhances the Nernst voltage and gas diffusion. To present some specific values, the

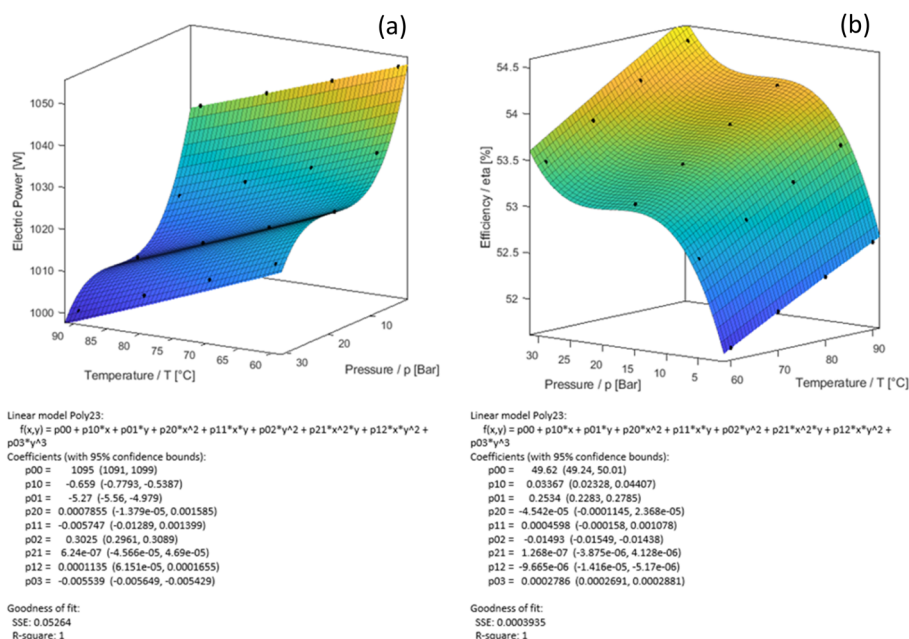


Fig. 13 PEMEL energy mapping. Gross electric power absorbed (a), conversion (system) efficiency (b).



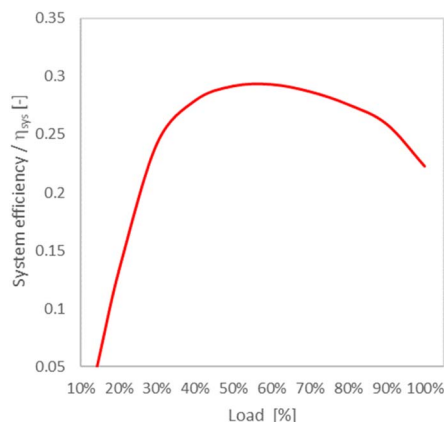


Fig. 14 Overall H2PEM system efficiency vs. load.

minimum electric power delivered occurs at 1 bar and 60 °C, with a value close to 600 W. The maximum electric power is achieved at 90 °C and 30 bar, where it more than doubles, reaching over 1200 W. Other values can be easily extracted from chart (a). When examining the system efficiency of the fuel cell unit, a distinct pattern emerges. The efficiency curve exhibits an 'S' shape with respect to pressure and a 'U' shape with respect to temperature. As known, pressure is generally beneficial for efficiency, but its effect diminishes at higher temperatures. At lower temperatures (60 °C), the highest efficiency (close to 43%) is observed at the highest pressure. However, at higher temperatures (90 °C), the highest efficiency occurs not at the highest pressure, but around 20 bar, where the efficiency approaches a value slightly above 43%. This is due to the less pronounced effect of temperature on efficiency at higher pressures. The 'U' shape effect due to temperature is attributed to the energy required to heat the incoming fluids into the PEMFC. At lower temperatures (60 °C), the energy expenditure for heating the fluids is minimal, resulting in a beneficial effect on efficiency. Conversely, as the temperature increases, the energy required to heat the fluids becomes more significant, which reduces the efficiency. At approximately 75 °C (1 bar), the lowest efficiency is observed. However, as the temperature continues to rise, the energy gain from the higher temperature exceeds the energy loss, and the efficiency begins to increase again.

Fig. 13 presents similar analyses for the electrolysis unit in chart form. From a thermo-electrochemical perspective, the trends observed are consistent with those seen in the fuel cell unit. As shown in chart (a), the electric power required by the electrolysis unit to produce hydrogen increases as the temperature decreases. This is because the energy expenditure due to overpotentials outweighs the benefit gained from lower heat loss during water heating. As is well-known in theory, higher pressures reduce the electric power absorption. The most challenging operating condition in the assessed range occurs at 1 bar and 60 °C, where the electric power demand exceeds 1050 W. Conversely, the optimal condition is at 90 °C and 30 bar, where the power requirement drops significantly, staying below 1000 W. In chart (b), the conversion efficiency of the electrolyzer follows a similar pattern to the power absorption.

Under the worst condition (1 bar, 60 °C), the conversion efficiency is approximately 51.5%. At the best condition (30 bar, 90 °C), the efficiency approaches 55%.

Another insightful analysis involves presenting the overall energy efficiency of the H2PEM system as a function of the load. In this context, load refers to the current electric power exchanged (either incoming or outgoing) divided by the maximum value (approximately 1 kW). Fig. 14 illustrates this relationship. As seen in the chart, the overall H2PEM efficiency profile follows a parabolic curve, which flattens in the central region of the loads. This chart is valuable because it highlights the operational load ranges where inefficiencies are minimized and where the H2PEM power station likely delivers its best performance. Specifically, it can be concluded that within the load range of 30–90%, the H2PEM efficiency remains above 25%. The highest efficiency, approximately 30%, is observed around 55% of the load.

An analysis of the findings reveals that they are consistent with those reported in the literature and examined in this study.^{10,107,127}

Dynamic energy analysis

The dynamic simulations are designed to evaluate the system's response to fluctuations in external electric power, specifically surplus or deficits in the network. The aim of this paper is to validate the tool, so the simulations involve a random signal representing positive (surplus: $\Delta P+$) and negative (deficit: $\Delta P-$) power variations, which reflect the characteristics of an energy network predominantly powered by renewable sources. The simulations are conducted over a period of 90 000 seconds, with hypothesis of power variations occurring in cycles of 3600 seconds.

Fig. 15 illustrates the dynamics of the H2PEM power station, including: (a) the Δ power inputs, (b) the state SOC of the MHD and H2C, (c) the power response of the PEMFC, (d) the dynamics of hydrogen consumption and production, (e) the power response of the PEMEL, and (f) the energy efficiency. Generally, the activation of the electrolyzer corresponds to power surpluses, while the activation of the fuel cell corresponds to power deficits. However, this pattern may vary due to the control logic, which considers both SOC limits and the operational constraints of the electrolyzer and fuel cell. For example, if the power surplus does not exceed the auxiliary power requirements of the electrolyzer plus a safety threshold, the control logic may not activate the electrolyzer.

Analogously, the fuel cell is activated if the power to be compensated is higher than its auxiliary absorption. The fuel cell can compensate for power deficits up to its maximum nominal power. Additionally, the system's operation is constrained by the SOC of the hydrogen storage units. The minimum SOC for MHD storage is set at 30%, while for the H2C storage, it is set at 50%. As depicted in Fig. 15b, the primary role in meeting power demands is fulfilled by the MHD, with the H2C providing supplementary support once the MHD reaches its minimum SOC (around 10 000 seconds). When both the MHD and H2C storage units hit their minimum SOC levels, the



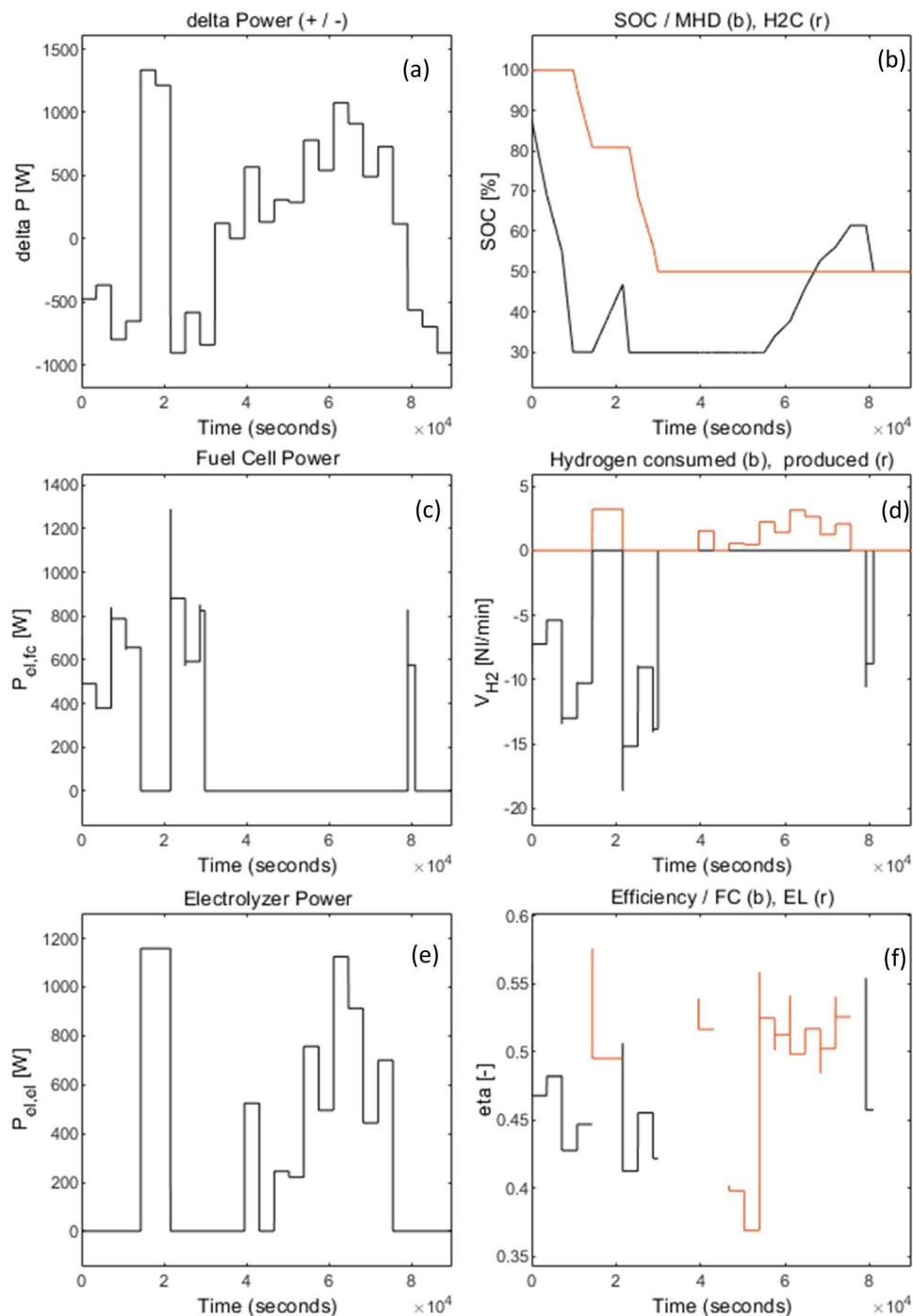


Fig. 15 Dynamic simulations – (b): black, (r): red. Electric power variation (a), SOC of H_2 reservoirs (b), fuel cell power (c), consumption and production of H_2 (d), electrolyzer power (e), fuel cell and electrolyzer efficiency (f).

H_2PEM system can no longer address power shortages and must wait for a power surplus to regenerate hydrogen pressure. This scenario is evident between 30 000 and 50 000 seconds. By approximately 50 000 seconds, the MHD tank has been repressurized. The control logic allows the H_2C to be repressurized when the MHD reaches 100% SOC. Consequently, hydrogen from the MHD is used to meet electric power requests, as observed around 80 000 seconds. Fig. 15 f illustrates the efficiency of the machines, with the PEMFC efficiency fluctuating

around 45%, peaking above 50%, while the PEMEL efficiency averages 50%, with peaks exceeding 55%.

Within the broader context of the energy transition, the network would predominantly rely on renewable sources. It should be emphasized that the numerical tool has successfully been tested for rapid electric load variations, demonstrating how the system effectively responds to rapid electric load changes, occurring within seconds.¹⁹³



Table 5 Parameters for environmental analysis

Scenario	Energy share	Fossil ^a	Solar	Wind	Hydro
1	Fossil	100%	—	—	—
2	Share (Italy 2023)	72.2%	4.83%	9.8%	13.18%
3	All renewable	—	17.4%	35.2%	47.4%
CO ₂ equivalent emission factor [kg _{CO₂,eq} MW ⁻¹ h ⁻¹]		307.7	48	11	24
Reference →		195	184	184	184

^a Fossil-based energy is intended as thermal power plant fed by natural gas.

Table 6 Specific results of the environmental analysis

Scenario	Energy share	CO ₂ emissions [kg _{CO₂} kg _{H₂} ⁻¹]	Fuel used [kg _{fuel} kg _{H₂} ⁻¹]	Temperature increase ΔT [°C ppm _{CO₂} ⁻¹]
1	Fossil	93.36	11.74	10.5×10^{-3}
2	Share (Italy 2023)	14.91		
3	All renewable	1.539		

CO₂ emissions and climate-change related implications

This section presents the results of the environmental analysis for the three hypothesized scenarios. For the benefit of the reader, the scenarios are repeated.

Scenario 1: hydrogen is produced using electricity sourced entirely from the grid, with the assumption that all energy comes from fossil fuels.

Scenario 2: hydrogen production relies on electricity from the Italian grid. According to the “TERNA Driving Energy” report (TERNA is the operator of the Italian high and very high voltage electricity transmission network – <https://www.terna.it/>), the energy mix for 2023 was as follows: 72.2% from fossil fuels (primarily natural gas power plants), 4.83% from solar photovoltaic plants, 9.8% from wind energy, and 13.18% from hydroelectric power plants.

Scenario 3: hydrogen is produced using a network powered entirely by renewable energy. This scenario assumes that fossil energy is completely phased out, with the energy mix being fully renewable.

Table 5 lists the parameters used, including the energy share and the CO₂ emission factors for each energy source. CO₂ emission factors are taken from highly reputed documents. The CO₂ emission factor for the Italian power plants (powered by natural gas) is taken from the official report “Emission factors for electricity production and consumption in Italy, 2024” of the Italian Institute for Environmental Protection and Research.¹⁹⁵ Regarding the renewable energy plants, the CO₂ emission factors of Solar, Wind and Hydro power plants, are taken from the recent study (2023) of Aghakhani *et al.*¹⁸⁴ It is very important to underline that in all cases the CO₂ emission factor must be intended as CO₂ equivalent, thus including the effects of the other known greenhouse gases, such as methane and oxides of nitrogen. These values consider the entire life cycle of the plants, including the energy used for the construction.

Based on the above premises, the CO₂ emission factors of the natural gas-powered plants is equal to about 308 kg_{CO₂,eq} MW⁻¹ h⁻¹. The emission factors of solar, wind and hydro power plants are respectively: 48, 11, 24 kg_{CO₂,eq} MW⁻¹ h⁻¹.

Table 6 details the specific results of the environmental analysis, including CO₂ emissions per kilogram of hydrogen

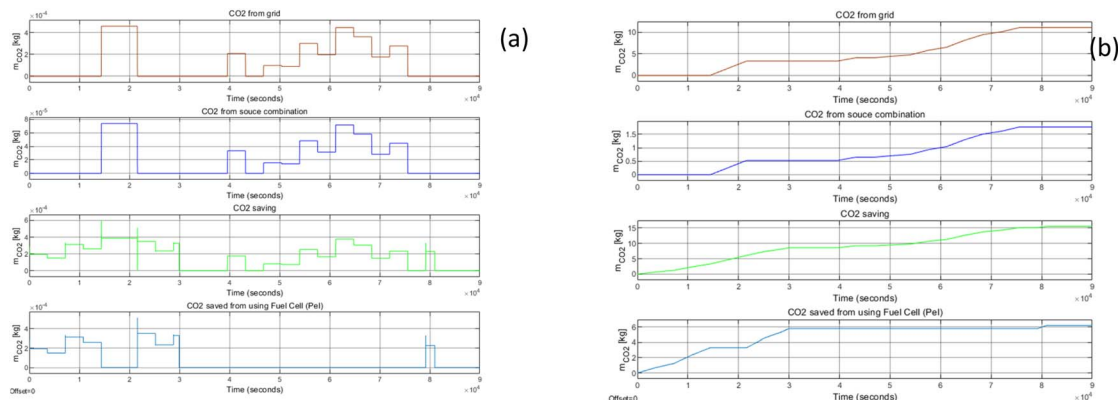


Fig. 16 CO₂ emissions and saving: (a) instantaneous, (b) cumulated. Comparison between scenario 1 and 2.



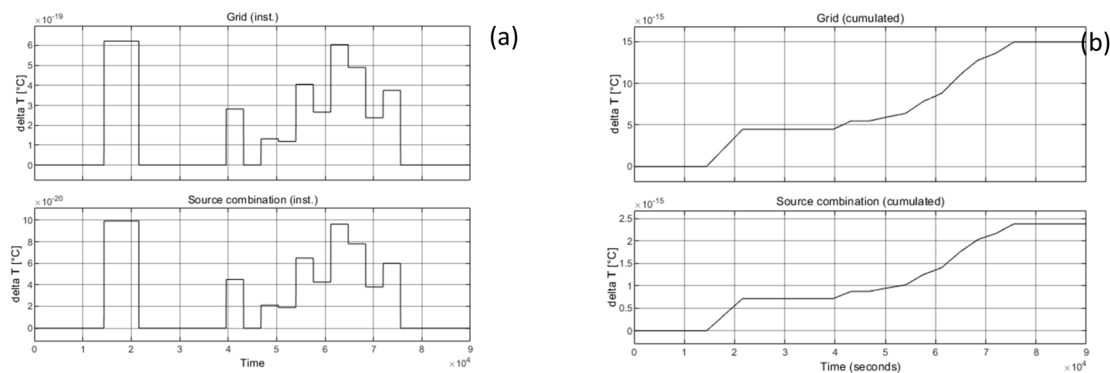


Fig. 17 Climate change: temperature increase associated to CO₂ emissions. (a) instantaneous, (b) cumulated. Comparison between scenario 1 and 2.

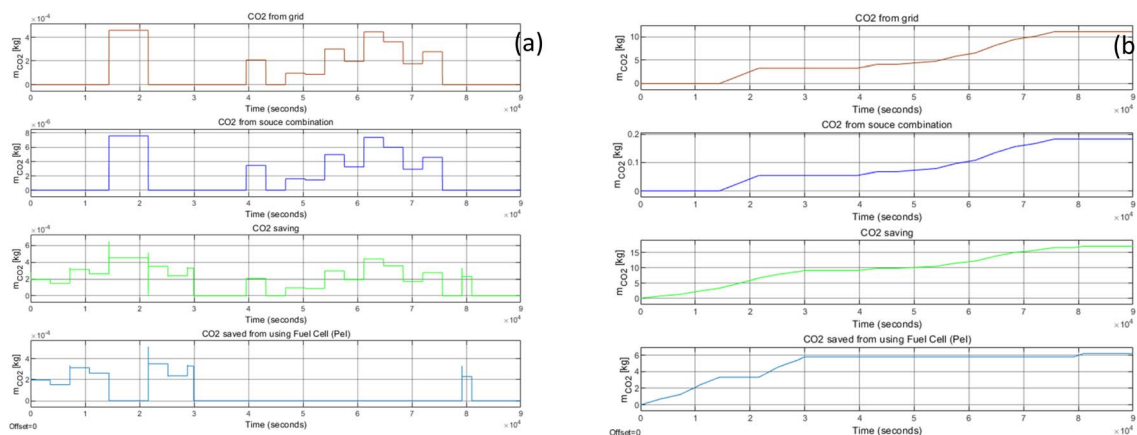


Fig. 18 CO₂ emissions and savings: (a) instantaneous, (b) cumulated. Comparison between scenario 1 and 3.

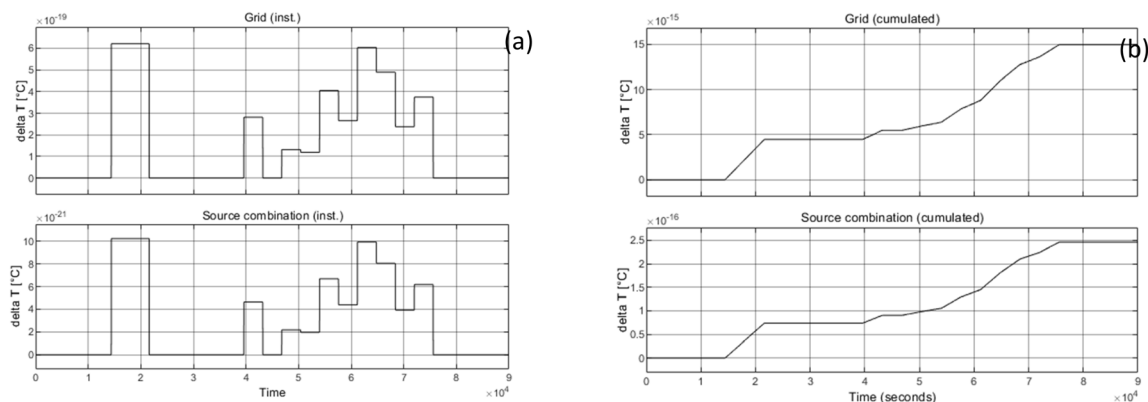


Fig. 19 Climate change: temperature increase associate to CO₂ emissions. (a) instantaneous, (b) cumulated. Comparison between scenario 1 and 3.

produced for each scenario. In Scenario 1, where hydrogen is produced entirely using electricity from fossil fuels, CO₂ emissions amount to 93.36 kg_{CO2} kg_{H2}⁻¹. In Scenario 2, which reflects the energy mix in Italy for 2023, CO₂ emissions decrease to 14.91 kg_{CO2} kg_{H2}⁻¹. The most favorable Scenario 3, utilizing

only renewable energy sources, reduces CO₂ emissions to 1.539 kg_{CO2} kg_{H2}⁻¹. The analysis also calculates the temperature increase associated with CO₂ concentration changes, showing a rise of 10.5×10^{-3} °C per ppm of CO₂ emitted into the atmosphere. This result is consistent with experimental



evidence, showing a temperature change of approximately 0.1°C for every 10 ppm increase in CO_2 concentration.

Fig. 16–19 display simulations conducted over 90 000 seconds to better illustrate system dynamics, including both instantaneous and cumulative values. These figures indicate that by the end of the simulations, the H2PEM power station can avoid approximately 15 kg of CO_2 when powered by the energy mix of Scenario 2 (green chart in Fig. 16(b)). Scenario 3 achieves a greater reduction, avoiding more than 17 kg of CO_2 (green chart in Fig. 18(b)). Comparing temperature increases, Scenario 1 results in a ΔT of about $15 \times 10^{-15}^\circ\text{C}$ (Fig. 17(b)), Scenario 2 results in ΔT of approximately $2.4 \times 10^{-15}^\circ\text{C}$, and Scenario 3 shows a ΔT of only $2.5 \times 10^{-16}^\circ\text{C}$ (Fig. 19(b)). This demonstrates a reduction of 60 times when transitioning from fossil to renewable energy sources.

For a more comprehensive analysis, it is important to consider existing technologies in similar applications, particularly in integrated electric networks. Conventional and mature technologies, such as Internal Combustion Engines (ICE) and Gas Turbines (GT), should be included in this context. While these technologies are still far from being fully compatible and mature with hydrogen, some research papers provide both numerical and experimental studies on their potential use with hydrogen. In a realistic scenario, ICEs and GTs would be fueled with natural gas from the existing distributed infrastructure. In such cases, the analysis becomes straightforward, with the CO_2 emission factor chosen to correspond to ICEs and GTs operating on natural gas.

Conclusions

This paper presented the development of a numerical tool devoted to energy and environmental assessment, when a 1 kW-H2PEM power station interacts with a superior energy network. Central to this endeavor was the deployment of a robust hydrogen storage entity, engineered to bolster system reliability and adaptability. The H2PEM is composed of a PEM fuel cell (PEMFC), PEM electrolyzer (PEMEL), compression (H2C) and metal hydride (MHD) storage reservoirs.

A series of simulations was conducted to characterize the system's energy performance and dynamics. The results revealed a nominal electric efficiency of 40.5% for the fuel cell system and 55% for the electrolysis unit, operating at pressures of 6 and 16 bar, respectively. The modeling framework is regulated to maintain a constant temperature (conventionally 80°C) carefully analyzing heat exchange dynamics required by fluctuations in electric current. The system is managed by a control logic that accounts for technical and operational constraints, including SOC limits and the operating conditions of both the electrolyzer and the fuel cell. The MHD plays a primary role in meeting power demands, while the H2C provides additional support once the MHD reaches its minimum SOC. When both the MHD and H2C storage units reach their minimum SOC levels, the H2PEM system cannot address power shortages and must await a power surplus to regenerate hydrogen pressure in tanks.

A comprehensive energy analysis was conducted to map the overall performance of the H2PEM power station, identifying

the most favorable operating conditions for achieving high system efficiency.

The tool was also dynamically tested with random-variable electric power inputs over a simulation period of 90 000 seconds to assess the system's robustness and resilience. The results showed that the PEMFC efficiency varied around 45%, with peaks exceeding 50%, while the PEMEL efficiency averaged 50%, with peak values surpassing 55%.

The environmental analysis, which examines CO_2 production and related temperature changes, was conducted under three scenarios: (1) electrolysis powered by electricity from a fossil-fuel-based grid, (2) electrolysis powered by the electricity grid based on Italy's 2023 energy mix, and (3) electrolysis powered entirely by renewable energy sources (composed of solar, wind, and hydro plants according to 2023 Italy's renewables' share). In Scenario 1, CO_2 emissions amount to $93.36 \text{ kg}_{\text{CO}_2} \text{ kg}_{\text{H}_2}^{-1}$. Scenario 2, reflecting the 2023 Italian energy mix, reduces CO_2 emissions to $14.91 \text{ kg}_{\text{CO}_2} \text{ kg}_{\text{H}_2}^{-1}$.

The most favorable Scenario 3, utilizing solely renewable sources, reduces CO_2 emissions further to $1.539 \text{ kg}_{\text{CO}_2} \text{ kg}_{\text{H}_2}^{-1}$. The temperature increase associated with CO_2 concentration changes is $10.5 \times 10^{-3}^\circ\text{C}$ per ppm of CO_2 emitted into the atmosphere. Dynamic analysis, using random power exchange conditions over 90 000 seconds, showed that the H2PEM power station can avoid approximately 15 kg of CO_2 with the energy mix of Scenario 2 and more than 17 kg of CO_2 with Scenario 3. Temperature increase comparisons reveal that Scenario 1 results in a ΔT of about $15 \times 10^{-15}^\circ\text{C}$, Scenario 2 yields ΔT of approximately $2.4 \times 10^{-15}^\circ\text{C}$, and Scenario 3 results in a ΔT of only $2.5 \times 10^{-16}^\circ\text{C}$.

Future work will enhance the numerical tool by integrating a comprehensive model of the overarching energy network, including components such as photovoltaic systems, wind turbines, the electricity grid, and battery storage, all of which will supply a potential user. Additionally, a comprehensive environmental impact life cycle assessments will be developed according to structures and material used for such systems.

Future research directions

Building upon the findings of this study, future work could explore the integration of additional renewable energy sources such as biomass, wind, geothermal power (even the low-quality heat technology of the Organic Rankine Cycle) into and together the H2PEM system, further enhancing its flexibility and sustainability. Additionally, investigating different configurations of the hydrogen storage system, such as hybrid systems combining metal hydride storage with compressed gas storage, could offer new insights into improving system performance and resilience. The development of a more advanced control logic, capable of optimizing energy management across diverse renewable inputs, would also contribute to improving the operational efficiency of the system. Finally, long-term experimental validation of the model's predictions under real-world conditions could help to refine the system's performance and robustness, providing more reliable guidance for large-scale deployment.



Symbology

Table 7 includes definitions and explanations of the symbols used in this paper.

Table 7 Symbology

Symbol	Unit of measure	Meaning
General		
P	W	Power
C_t	J K^{-1}	Thermal capacity
P_{in}	W	Generic input power
P_{out}	W	Generic output power
p	bar	Pressure
p_0	bar	Reference pressure
T	$^{\circ}\text{C}$	Temperature
n_e	—	Number of electrons
F_a	C mol^{-1}	Faraday constant
\mathfrak{R}	$\text{J mol}^{-1} \text{K}^{-1}$	Gas constant
n_c	—	Number of cell
$P_{\text{blow}}^{\text{cool}}$	W	Generic electric power for blower working
$\dot{V}_{\text{air}}^{\text{cool}}$	Nl min^{-1}	Flowrate of generic air cooling
Δp_{tot}	bar	Pressure losses
η_{blow}	—	Blower efficiency
$P_{\text{fluid}}^{\text{warm}}$	W	Generic electric power for fluid warming
$\eta_{\text{el}}^{\text{warm}}$	—	Electric efficiency of generic electric warmer
$F_{\text{fluid}}^{\text{in}}$	mol s^{-1}	Flowrate of generic input fluid
$\Delta \bar{h}_{\text{fluid}}^{\text{in}}$	J mol^{-1}	Enthalpy of generic input fluid
$P_{\text{fc/el}}^{\text{(el-warm)}}$	W	Generic electric power for device warming
$m_{\text{fc/el}}$	kg	Generic mass of device
c_p	$\text{J mol}^{-1} \text{K}^{-1}$	Specific heat
ΔT	$^{\circ}\text{C}$	Temperature variation
FW	—	Friction factor
ε_a	mm	Absolute rugosity
d_{eq}	mm	Equivalent diameter
ν	$\text{m}^2 \text{s}^{-1}$	Cinematic viscosity
ρ	kg m^{-3}	Mass density
r_{co}	—	Factor for distributed head losses calculation
Δp_d	bar	Distributed pressure losses
n_l	—	Number of channels
l_{air}	cm	Length of channel
Δp_c	bar	Concentrated pressure losses
χ	—	Factor for concentrated head losses calculation
c_{air}	m s^{-1}	Air velocity
C	Farad	Capacity
R_{an}	Ω	Anodic resistance
R_{mem}	Ω	Electrolyte resistance
R_{cat}	Ω	Cathodic resistance
V_{real}	V	Real voltage at terminals
V_{an}	V	Anodic voltage
V_{cat}	V	Cathodic voltage
V_{int}	V	Internal voltage
i	A	Electric dynamic current
$E_{\text{H}_2}^{\text{s}}(t)$	J	Hydrogen energy stored at time t
$E_{\text{H}_2}^{\text{max}}$	J	Maximum hydrogen energy stored



Table 7 (Contd.)

Symbol	Unit of measure	Meaning
$SOC(t)$	— or %	State of charge of H_2 storage unit
f_{FC}^{ampl}	—	Amplification factor in fuel cell
f_{EL}^{ampl}	—	Amplification factor in electrolyzer
ΔP^{fc-}	W	Electric power to be erogated by the fuel cell unit
ΔP^{el+}	W	Electric power to be absorbed by the electrolysis unit
$Q, E, \varepsilon_0, s, d$		Parameters related to capacitance calculation (eqn (6))
$\frac{d... (t)}{dt}$		Time derivative
Fuel cell		
V_c^{fc}	V	Single cell voltage
E_{N_fc}	V	Nernst voltage
A	—	Modeling parameter in activation
j^{fc}	$A\ cm^{-2}$	Electric current density
j_n	$A\ cm^{-2}$	Electric current density
j_0	$A\ cm^{-2}$	Exchange electric current density
j_L	$A\ cm^{-2}$	Limiting electric current density
ASR	$\Omega\ cm^{-2}$	Area specific resistance
B	—	Modeling parameter in concentration
i^{fc}	A	Electric current
$A_{c,fc}$	cm^2	Active surface
$P_{th}^{(p)}$	W	Produced thermal power
$\Delta \tilde{g}_{fc}^0(T, p_0)$	$J\ mol^{-1}$	Gibbs free energy variation for fuel cell
$\Delta \tilde{h}_{r,H_2}$	$J\ mol^{-1}$	Electrochemical reaction
$\lambda_{H_2,fc}$	—	Hydrogen supply excess factor
$\lambda_{O_2,fc}$	—	Oxygen supply excess factor
\dot{V}_{an}^{out}	$Nl\ min^{-1}$	Output anodic flowrate
\dot{V}_{cat}^{out}	$Nl\ min^{-1}$	Output cathodic flowrate
$\dot{V}_{H_2}^{(r)}$	$Nl\ min^{-1}$	Reacted hydrogen flowrate
$\dot{V}_{O_2}^{(r)}$	$Nl\ min^{-1}$	Reacted oxygen flowrate
$\dot{V}_{H_2O}^{(p)}$	$Nl\ min^{-1}$	Produced water flowrate
$\dot{V}_{H_2}^{(in)}$	$Nl\ min^{-1}$	Input hydrogen flowrate
\dot{V}_{air}^{in}	$Nl\ min^{-1}$	Input air flowrate
$P_{FC}^{stack(gross)}$	W	Stack gross electric power
$P_{el}^{(p)}$	W	Produced electric power
$P_{DC/DC}^{(net,out)}$	W	Net electric power at DC/DC terminals
$\Delta P_{DC/DC}^{(out)}$	W	Power loss at DC/DC
$P_{AIR}^{(sup)}$	W	Electric power for air supply
$P_{AIR}^{(cool)}$	W	Electric power for air cooling
$P_{fc}^{(el-warm)}$	W	Electric power for fuel cell warming
$P_{in-gas}^{(warm)}$	W	Electric power for entering gas heat-up
$P_{blow}^{air,in}$	W	Electric power for blow working
η_{el}^{fc}	— or %	Electric efficiency
$F_{H_2}^{in}$	$mol\ s^{-1}$	Hydrogen input flowrate
$\Delta \tilde{h}_{H_2}^{in}$	$J\ mol^{-1}$	Hydrogen input enthalpy
F_{Air}^{in}	$mol\ s^{-1}$	Air supply input flowrate
$\Delta \tilde{h}_{Air}^{in}$	$J\ mol^{-1}$	Air supply input enthalpy
V_{tn}^{fc}	V	Thermoneutral voltage of the fuel cell stack
V_{st}^{fc}	V	Voltage of the fuel cell stack
$F_{Air}^{in,cool}$	$mol\ s^{-1}$	Air cooling input flowrate



Table 7 (Contd.)

Symbol	Unit of measure	Meaning
$\Delta \tilde{h}_{\text{Air}}^{\text{in,cool}}$	J mol^{-1}	Air cooling input enthalpy
$F_{\text{H}_2\text{O}}^{\text{out}}$	mol s^{-1}	Output water flowrate
$\Delta \tilde{h}_{\text{H}_2\text{O}}^{\text{out}}$	J mol^{-1}	Output water enthalpy
$F_{\text{Air}}^{\text{out}}$	mol s^{-1}	Output air supply flowrate
$\Delta \tilde{h}_{\text{Air}}^{\text{out}}$	J mol^{-1}	Output air supply enthalpy
$F_{\text{Air}}^{\text{out,cool}}$	mol s^{-1}	Output air cooling flowrate
$\Delta \tilde{h}_{\text{Air}}^{\text{out,cool}}$	J mol^{-1}	Output air cooling enthalpy
Electrolyzer		
V_{c}^{el}	V	Single cell voltage
$E_{\text{N,el}}$	V	Nernst voltage
i^{el}	A	Electric current
$A_{\text{c,el}}$	cm^2	Active surface
$P_{\text{th}}^{\text{(gen)}}$	W	Generated thermal power
$\Delta \tilde{g}_{\text{el}}^0(T, p_0)$	J mol^{-1}	Gibbs free energy variation for fuel cell
$\Delta \tilde{h}_{\text{r,H}_2\text{O}}$		Electrochemical reaction
λ_{el}	—	Water supply excess factor
$\dot{V}_{\text{cat}}^{\text{out}}$	Nl min^{-1}	Output cathodic flowrate
$\dot{V}_{\text{an}}^{\text{out}}$	Nl min^{-1}	Output anodic flowrate
$\dot{V}_{\text{O}_2}^{(\text{p})}$	Nl min^{-1}	Produced oxygen flowrate
$\dot{V}_{\text{H}_2\text{O}}^{(\text{in})}$	Nl min^{-1}	Input water flowrate
$\dot{V}_{\text{H}_2\text{O}}^{(\text{r})}$	Nl min^{-1}	Reacted water flowrate
$P_{\text{EL}}^{\text{stack(net)}}$	W	Net electric power at stack terminals
$P_{\text{el}}^{(\text{us})}$	W	Used/absorbed electric power
$P_{\text{DC/DC}}^{(\text{gross,in})}$	W	Gross electric power at DC/DC terminals
$\Delta P_{\text{DC}}^{(\text{in})}$	W	Power loss at DC/DC
$P_{\text{AIR}}^{(\text{cool})}$	W	Electric power for air cooling
$P_{\text{H}_2\text{O}}^{(\text{warm})}$	W	Electric power for entering water heat-up
$P_{\text{el}}^{(\text{el-warm})}$	W	Electric power for warming
$\eta_{\text{H}_2}^{\text{el}}$	— or %	Hydrogen production efficiency
$F_{\text{H}_2\text{O}}^{\text{in}}$	mol s^{-1}	Water input flowrate
$\Delta \tilde{h}_{\text{H}_2\text{O}}^{\text{in}}$	J mol^{-1}	Water input enthalpy
$F_{\text{Air}}^{\text{in,cool}}$	mol s^{-1}	Air cooling input flowrate
$\Delta \tilde{h}_{\text{Air}}^{\text{in,cool}}$	J mol^{-1}	Air cooling input enthalpy
$V_{\text{tn}}^{\text{el}}$	V	Thermoneutral voltage of the stack
$V_{\text{st}}^{\text{fc}}$	V	Voltage of the stack
$F_{\text{H}_2}^{\text{out}}$	mol s^{-1}	Output hydrogen flowrate
$\Delta \tilde{h}_{\text{H}_2}^{\text{out}}$	J mol^{-1}	Output hydrogen enthalpy
$F_{\text{O}_2}^{\text{out}}$	mol s^{-1}	Output oxygen flowrate
$\Delta \tilde{h}_{\text{O}_2}^{\text{out}}$	J mol^{-1}	Output oxygen enthalpy
$F_{\text{Air}}^{\text{out,cool}}$	mol s^{-1}	Output air cooling flowrate
$\Delta \tilde{h}_{\text{Air}}^{\text{out,cool}}$	J mol^{-1}	Output air cooling enthalpy
Hydrogen compression tank – H2C		
$p_{\text{H}_2\text{C}}(t)$	Pa	Pressure of hydrogen in H2C at time t
V_{tank}	m^3	Tank volume
$m_{\text{H}_2}(t)$	kg	Hydrogen stored at time t
z	—	Factor for real gas



Table 7 (Contd.)

Symbol	Unit of measure	Meaning
MW_{H_2}	$g\ mol^{-1}$	
$E_{H_2}^{s,H_2C}(t)$	J	Hydrogen energy stored at time t
$E_{H_2}^{s,max,H_2C}$	J	Maximum hydrogen energy stored at time t
LHV_{H_2}	$J\ g^{-1}$	
Hydrogen metal hydride tank – MHD		
p_{MHD}	bar	Pressure
p_{eq}	bar	Equilibrium pressure
La_*	—	Lacher function
$\Delta h_{r,MHD}$	$J\ mol^{-1}$	Reaction enthalpy in MHD
$\Delta s_{r,MHD}$	$J\ mol^{-1}\ K^{-1}$	Reaction entropy in MHD
T_{MHD}	°C	Working temperature
T_c	°C	Critical temperature
θ	—	Concentration ratio
$\alpha_1, \alpha_2, n_1, n_2, k_1, k_2$	—	Modeling parameters
$c(t)$	—	Hydrogen concentration at time t
c_{max}	—	Maximum hydrogen concentration
$m_{H_2,MHD}(t)$	kg	Hydrogen mass stored at time t
$m_{H_2,MHD}^{max}$	kg	Maximum mass energy stored
$E_{H_2}^{s,MHD}(t)$	J	Hydrogen energy stored at time t
$E_{H_2}^{s,max,MHD}$	J	Maximum hydrogen energy stored
Enviromental analysis and climate change implications		
$X_{CO_2}^{grid}$	$kg_{CO_2}\ kg_{H_2}^{-1}$	CO ₂ emissions associated to electrolysis entirely powered by fossil energy
	$t\ kg^{-1}$	1×10^{-3}
m_f^s	$kg_f\ kg_{H_2}^{-1}$	Specific mass flow rate of fuel
LHV_f	$GJ\ t^{-1}$	Low heart value of fossil fuel
e_f^{fa}	$kg_{CO_2}\ GJ^{-1}$	CO ₂ emission factor
	$(GJ/t)\ (kg/kW\ h)^{-1}$	3.6
η_{el}^f	—	Electric efficiency of power plant fed by fossil fuel
$E_{H_2}^s$	$kW\ h\ kg_{H_2}^{-1}$	Specific electric energy of electrolysis
$X_{CO_2}^{comb}$	$kg_{CO_2}\ kg_{H_2}^{-1}$	CO ₂ emissions associated to combustion of fossil fuel
C_s, C_w, C_h, C_o	% MW h	Energy share (solar, wind, hydro, rest)
E_s, E_w, E_h, E_o	$kg_{CO_2}\ MW^{-1}\ h^{-1}$	CO ₂ emission factor per energy source
S	°C	Climate sensitivity factor
$c_0, \Delta c$	ppm	Initial and delta concentration of CO ₂
$\Delta T(c)$	°C	Temperature variation (increase)

Data availability

The data used for the validation of the tool can be consulted *via* the associated reference. The code of this work was developed in-house using the Matlab/Simulink environment on Matlab version 2022a. All results are generated *via* code executions and are presented as graphs.

Author contributions

Orlando Corigliano: conceptualization, methodology, software, validation, formal analysis, investigation, data curation, writing – original draft, writing – review & editing, visualization.

Petronilla Fragiaco: conceptualization, methodology, investigation, writing – original draft, writing – review & editing, visualization, supervision, project administration.

Conflicts of interest

There are no conflicts to declare.

Notes and references

- 1 M. Genovese, A. Schlüter, E. Scionti, F. Piraino, O. Corigliano and P. Fragiaco, *Int. J. Hydrogen Energy*, 2023, **48**, 16545–16568.



- 2 I. International Energy Agency, *The Future of Hydrogen*, 2019.
- 3 I. Renewable Energy Agency, *World Energy Transitions Outlook 2023: 1.5°C Pathway*, 2023.
- 4 I. International Energy Agency, *Global Hydrogen Review 2022*, 2022.
- 5 J. E. Garzón Baquero and D. Bellon Monsalve, *Int. J. Hydrogen Energy*, 2024, **54**, 574–585.
- 6 Z. Abdin, N. Al Khafaf, B. McGrath, K. Catchpole and E. Gray, *Sustain. Energy Fuels*, 2023, **7**, 2042–2062.
- 7 T. Grube, L. Doré, A. Hoffrichter, L. E. Hombach, S. Rath, M. Robinius, M. Nobis, S. Schiebahn, V. Tietze, A. Schnettler, G. Walther and D. Stolten, *Sustain. Energy Fuels*, 2018, **2**, 1500–1515.
- 8 Communication From The Commission To The European Parliament, The Council, The European Economic And Social Committee And The Committee Of The Regions, *A Hydrogen Strategy for a Climate-Neutral Europe*, European Commission, Brussels, 8.7.2020 COM(2020) 301 final, https://energy.ec.europa.eu/system/files/2020-07/hydrogen_strategy_0.pdf.
- 9 Hydrogen Europe, *Strategic Research and Innovation Agenda Final Draft*, 2020.
- 10 Clean Hydrogen Joint Undertaking, *Strategic Research and Innovation Agenda 2021–2027*, 2022, https://www.clean-hydrogen.europa.eu/about-us/key-documents/strategic-research-and-innovation-agenda_en.
- 11 European Commission, European Clean Hydrogen Alliance, https://single-market-economy.ec.europa.eu/industry/industrial-alliances/european-clean-hydrogen-alliance_en, (accessed 5 February 2025).
- 12 Department of Economic and Social Affairs - Sustainable Development, THE 17 GOALS, <https://sdgs.un.org/goals>, (accessed 5 September 2024).
- 13 A. E. Karaca, A. M. M. I. Qureshy and I. Dincer, *J. Clean. Prod.*, 2023, **385**, 135706.
- 14 S. Aslam, S. Rani, K. Lal, M. Fatima, T. Hardwick, B. Shirinfar and N. Ahmed, *Green Chem.*, 2023, **25**, 9543–9573.
- 15 S. V. Venkatesan, A. Nandy, K. Karan, S. R. Larter and V. Thangadurai, *Electrochem. Energy Rev.*, 2022, **5**, 16.
- 16 L. Zhou and Y. Zhou, *Energy Convers. Manag.*, 2023, **277**, 116610.
- 17 K. Brinkert and P. Mandin, *Nat. Res.*, 2022, **52**.
- 18 L. Ge, B. Zhang, W. Huang, Y. Li, L. Hou, J. Xiao, Z. Mao and X. Li, *J. Energy Storage*, 2024, **75**, 109307.
- 19 J. G. Love, A. P. O'Mullane, F. A. Boulaire and I. D. R. Mackinnon, *Sustain. Energy Fuels*, 2022, **6**, 4008–4023.
- 20 S. G. Nnabuike, E. Oko, B. Kuang, A. Bello, A. P. Onwualu, S. Oyagha and J. Whidborne, *Sustain. Chem. Clim. Action*, 2023, **2**, 100024.
- 21 O. Dybiński, Ł. Szabłowski, A. Martsinchyk, A. Szczęśniak, J. Milewski, A. Grzebielec and P. Shuhayeu, *Energies*, 2025, **18**, 552.
- 22 IEA, *Global Hydrogen Review 2024*, Paris, 2024.
- 23 A. M. Sadeq, R. Z. Homod, A. K. Hussein, H. Togun, A. Mahmoodi, H. F. Islem, A. R. Patil and A. H. Moghaddam, *Sci. Total Environ.*, 2024, **939**, 173622.
- 24 B. C. Erdener, B. Sergi, O. J. Guerra, A. Lazaro Chueca, K. Pambour, C. Brancucci and B.-M. Hodge, *Int. J. Hydrogen Energy*, 2023, **48**, 5595–5617.
- 25 C. Peter, E. Vrettos and F. N. Büchi, *Int. J. Electr. Power Energy Syst.*, 2022, **141**, 108121.
- 26 Y. Wang, Y. Pang, H. Xu, A. Martinez and K. S. Chen, *Energy Environ. Sci.*, 2022, **15**, 2288–2328.
- 27 L. Zhang, T. Porter, S. Guillory, C. Chi and C. G. Arges, *ECS Trans.*, 2017, **77**, 1325–1335.
- 28 Y. S. Kim, *ACS Appl. Polym. Mater.*, 2021, **3**, 1250–1270.
- 29 M. Shaygan, M. A. Ehyaei, A. Ahmadi, M. E. H. Assad and J. L. Silveira, *J. Clean. Prod.*, 2019, **234**, 1082–1093.
- 30 A. Mayyas and M. Mann, *Procedia Manuf.*, 2019, **33**, 508–515.
- 31 H. Montazerinejad, E. Fakhimi, S. Ghandehariun and P. Ahmadi, *Sustain. Energy Technol. Assessments*, 2022, **51**, 101885.
- 32 B. B. Choi, J. H. Jo, Y. S. Yoo, S.-Y. Jeon, T. Lee, Y.-J. Choi, D. Y. Chung, E.-J. Lee and S. J. Yoo, *Sustain. Energy Technol. Assessments*, 2023, **57**, 103238.
- 33 S. M. Abu, M. A. Hannan, P. J. Ker, M. Mansor, S. K. Tiong and T. M. I. Mahlia, *J. Energy Storage*, 2023, **72**, 108773.
- 34 M. B. Hossain, M. R. Islam, K. M. Muttaqi, D. Sutanto and A. P. Agalgaonkar, *J. Energy Storage*, 2023, **62**, 106842.
- 35 F. Rahim Malik, H.-B. Yuan, J. C. Moran and N. Tippayawong, *Eng. Sci. Technol. Int. J.*, 2023, **43**, 101452.
- 36 W. Son, S. Lee and J. Woo, *Renew. Sustain. Energy Rev.*, 2023, **187**, 113778.
- 37 A. Alaswad, A. Omran, J. R. Sodre, T. Wilberforce, G. Pignatelli, M. Dassisti, A. Baroutaji and A. G. Olabi, *Energies*, 2020, **14**, 144.
- 38 S. Chakraborty, S. K. Dash, R. M. Elavarasan, A. Kaur, D. Elangovan, S. T. Meraj, P. Kasinathan and Z. Said, *Front. Energy Res.*, 2022, **10**, DOI: [10.3389/fenrg.2022.893475](https://doi.org/10.3389/fenrg.2022.893475).
- 39 K. Zhang, X. Liang, L. Wang, K. Sun, Y. Wang, Z. Xie, Q. Wu, X. Bai, M. S. Hamdy, H. Chen and X. Zou, *Nano Res. Energy*, 2022, **1**, e9120032.
- 40 K. W. Ahmed, M. J. Jang, M. G. Park, Z. Chen and M. Fowler, *Electrochem*, 2022, **3**, 581–612.
- 41 B. G. Gang and S. Kwon, *Int. J. Hydrogen Energy*, 2018, **43**, 6331–6339.
- 42 P. Fragiaco, M. Genovese, F. Piraino, O. Corigliano and G. De Lorenzo, *Machines*, 2022, **10**, 1121.
- 43 M. Bayat, M. Özalp and H. Gürbüz, *Sustain. Energy Technol. Assessments*, 2022, **52**, 102232.
- 44 X. Wang, J.-X. Wang, H. Zhang, S.-Y. Li and Y.-P. Cheng, *Sustain. Energy Fuels*, 2024, **8**, 322–346.
- 45 X. Ge, F. Zhang, L. Wu, Z. Yang and T. Xu, *Macromolecules*, 2022, **55**, 3773–3787.
- 46 L. A. King, M. A. Hubert, C. Capuano, J. Manco, N. Danilovic, E. Valle, T. R. Hellstern, K. Ayers and T. F. Jaramillo, *Nat. Nanotechnol.*, 2019, **14**, 1071–1074.



- 47 S. Hwang, H. Lee, Y.-G. Jeong, C. Choi, I. Hwang, S. Song, S. Y. Nam, J. H. Lee and K. Kim, *Int. J. Mol. Sci.*, 2022, **23**, 14252.
- 48 H. Teuku, I. Alshami, J. Goh, M. S. Masdar and K. S. Loh, *Int. J. Energy Res.*, 2021, **45**, 20583–20600.
- 49 T. Henriques, B. César and P. J. C. Branco, *Appl. Energy*, 2010, **87**, 1400–1409.
- 50 K. Ayers, *Curr. Opin. Chem. Eng.*, 2021, **33**, 100719.
- 51 W. H. Lee, Y.-J. Ko, J. H. Kim, C. H. Choi, K. H. Chae, H. Kim, Y. J. Hwang, B. K. Min, P. Strasser and H.-S. Oh, *Nat. Commun.*, 2021, **12**, 4271.
- 52 A. Lim, J. Kim, H. J. Lee, H.-J. Kim, S. J. Yoo, J. H. Jang, H. Young Park, Y.-E. Sung and H. S. Park, *Appl. Catal., B*, 2020, **272**, 118955.
- 53 M. Wappler, D. Unguder, X. Lu, H. Ohlmeyer, H. Teschke and W. Lueke, *Int. J. Hydrogen Energy*, 2022, **47**, 33551–33570.
- 54 F. Frieden and J. Leker, *Sustain. Energy Fuels*, 2024, **8**, 1806–1822.
- 55 M. A. Sattar, M. G. Rasul, M. I. Jahirul and M. M. Hasan, *Sustain. Energy Fuels*, 2024, **8**, 3545–3573.
- 56 D. Groppi, D. Astiaso Garcia, G. Lo Basso, F. Cumo and L. De Santoli, *Energy Convers. Manag.*, 2018, **177**, 64–76.
- 57 J. Andersson and S. Grönkvist, *Int. J. Hydrogen Energy*, 2019, **44**, 11901–11919.
- 58 A. G. Gebretatios, F. Banat and C. K. Cheng, *Sustain. Energy Fuels*, 2024, **8**, 5091–5130.
- 59 C. R. Matos, J. F. Carneiro and P. P. Silva, *J. Energy Storage*, 2019, **21**, 241–258.
- 60 H. Barthelemy, M. Weber and F. Barbier, *Int. J. Hydrogen Energy*, 2017, **42**, 7254–7262.
- 61 M. Aziz, A. T. Wijayanta and A. B. D. Nandiyanto, *Energies*, 2020, **13**, 3062.
- 62 Y.-P. Chen, S. Bashir and J. L. Liu, *Nanostructured Materials for Next-Generation Energy Storage and Conversion*, Springer Berlin Heidelberg, Berlin, Heidelberg, 2017.
- 63 S. Shafiee and M. H. McCay, *Int. J. Hydrogen Energy*, 2016, **41**, 9462–9470.
- 64 Y. Kojima, *Int. J. Hydrogen Energy*, 2019, **44**, 18179–18192.
- 65 M. Tang, S. Zhang and S. Chen, *Chem. Soc. Rev.*, 2022, **51**, 1529–1546.
- 66 N. Klopčič, I. Grimmer, F. Winkler, M. Sartory and A. Trattner, *J. Energy Storage*, 2023, **72**, 108456.
- 67 L. Mulky, S. Srivastava, T. Lakshmi, E. R. Sandadi, S. Gour, N. A. Thomas, S. Shanmuga Priya and K. Sudhakar, *Mater. Chem. Phys.*, 2024, **325**, 129710.
- 68 N. N. Nguyen, *Energy Fuels*, 2023, **37**, 9771–9789.
- 69 R. B. Ferreira, D. S. Falcão, V. B. Oliveira and A. M. F. R. Pinto, *J. Power Sources*, 2015, **277**, 329–342.
- 70 A. A. Shah, K. H. Luo, T. R. Ralph and F. C. Walsh, *Electrochim. Acta*, 2011, **56**, 3731–3757.
- 71 J. Zhao, X. Li, C. Shum and J. McPhee, *Energy and AI*, 2021, **6**, 100114.
- 72 M. Maier, K. Smith, J. Dodwell, G. Hinds, P. R. Shearing and D. J. L. Brett, *Int. J. Hydrogen Energy*, 2022, **47**, 30–56.
- 73 C. Siegel, *Energy*, 2008, **33**, 1331–1352.
- 74 X. Luo, C. Ren, J. Song, H. Luo, K. Xiao, D. Zhang, J. Hao, Z. Deng, C. Dong and X. Li, *J Mater Sci Technol*, 2023, **146**, 19–41.
- 75 H.-W. Wu, *Appl. Energy*, 2016, **165**, 81–106.
- 76 K. Xiong, W. Wu, S. Wang and L. Zhang, *Appl. Energy*, 2021, **301**, 117443.
- 77 D. S. Falcão and A. M. F. R. Pinto, *J. Cleaner Prod.*, 2020, **10**, DOI: [10.1016/j.jclepro.2020.121184](https://doi.org/10.1016/j.jclepro.2020.121184).
- 78 F. Yang, X. Xu, Y. Li, D. Chen, S. Hu, Z. He and Y. Du, *Energies*, 2023, **16**, 3547.
- 79 F. Aubras, C. Damour, M. Benne, M. Bessafi, C. Lin-Kwong-Chon, B. Grondin-Perez, J. Deseure and J. J. A. Kadjo, *ECS Meet. Abstr.*, 2020, **MA2020-02**, 3762.
- 80 S. Busquet, C. E. Hubert, J. Labbé, D. Mayer and R. Metkemeijer, *J. Power Sources*, 2004, **134**, 41–48.
- 81 O. Atlam and M. Kolhe, *Energy Convers. Manag.*, 2011, **52**, 2952–2957.
- 82 J. Jia, Y. Wang, Q. Li, Y. T. Cham and M. Han, *IEEE Trans. Energy Convers.*, 2009, **24**, 283–291.
- 83 D. Hao, J. Shen, Y. Hou, Y. Zhou and H. Wang, *Int. J. Chem. Eng.*, 2016, **2016**, 1–10.
- 84 T. M. Brown, J. Brouwer, G. S. Samuelsen, F. H. Holcomb and J. King, *J. Power Sources*, 2008, **182**, 240–253.
- 85 M. Koundi, H. El Fadil, Z. EL Idrissi, A. Lassoui, A. Intidam, T. Bouanou, S. Nady and A. Rachid, *Clean Technol.*, 2023, **5**, 531–568.
- 86 B. Abderezzak, B. Khelidj and M. Tahar Abbes, *Int. J. Hydrogen Energy*, 2014, **39**, 1593–1603.
- 87 K. Ettihir, L. Boulon, M. Becherif, K. Agbossou and H. S. Ramadan, *Int. J. Hydrogen Energy*, 2014, **39**, 21165–21176.
- 88 R. Guan and A. Bazylak, *Electrochim. Acta*, 2023, **447**, 142103.
- 89 K. Jing and C. Liu, *Energy Rep.*, 2023, **9**, 299–307.
- 90 A. Abbou and A. El Hassnaoui, *AIMS Energy*, 2022, **10**, 254–272.
- 91 A. A. El-Fergany, H. M. Hasanien and A. M. Agwa, *Energy Convers. Manag.*, 2019, **201**, 112197.
- 92 K. W. Harrison, E. Hernández-Pacheco, M. Mann and H. Salehfar, *J. Fuel Cell Sci. Technol.*, 2006, **3**, 220–223.
- 93 N. V. Dale, M. D. Mann and H. Salehfar, *J. Power Sources*, 2008, **185**, 1348–1353.
- 94 I. San Martín, A. Ursúa and P. Sanchis, *Energies*, 2014, **7**, 670–700.
- 95 Z. Abdin, C. J. Webb and E. M. A. Gray, *Int. J. Hydrogen Energy*, 2015, **40**, 13243–13257.
- 96 R. Escobar-Yonoff, D. Maestre-Cambronel, S. Charry, A. Rincón-Montenegro and I. Portnoy, *Heliyon*, 2021, **7**, e06506.
- 97 Z. Abdin, C. J. Webb and E. M. A. Gray, *Energy*, 2016, **116**, 1131–1144.
- 98 Y. Cao, Y. Li, G. Zhang, K. Jermisittiparsert and N. Razmjoooy, *Energy Rep.*, 2019, **5**, 1616–1625.
- 99 Á. Hernández-Gómez, V. Ramirez, D. Guilbert and B. Saldivar, *Renew. Energy*, 2021, **163**, 1508–1522.



- 100 H. M. Sultan, A. S. Menesy, A. Korashy, M. S. Hassan, M. H. Hassan, F. Jurado and S. Kamel, *Sustain. Energy Technol. Assessments*, 2024, **64**, 103673.
- 101 D. Zhang, Y. Yang, J. Fang and A. Alkhayyat, *Sustain. Energy Technol. Assessments*, 2022, **53**, 102401.
- 102 D. Shapiro, J. Duffy, M. Kimble and M. Pien, *Sol. Energy*, 2005, **79**, 544–550.
- 103 D. Ferrero and M. Santarelli, *Energy Convers. Manag.*, 2017, **148**, 16–29.
- 104 Ø. Ulleberg, T. Nakken and A. Eté, *Int. J. Hydrogen Energy*, 2010, **35**, 1841–1852.
- 105 F. Gallardo, J. García, A. Monforti Ferrario, G. Comodi and J. N. W. Chiu, *Int. J. Hydrogen Energy*, 2022, **47**, 27303–27325.
- 106 W. Nsour, T. Taa'mneh, O. Ayadi and J. AlAsfar, *J. Ecol. Eng.*, 2019, **20**, 1–10.
- 107 J. J. Caparrós Mancera, F. Segura Manzano, J. M. Andújar, F. J. Vivas and A. J. Calderón, *Electronics*, 2020, **9**, 871.
- 108 L. Gracia, P. Casero, C. Bourasseau and A. Chabert, *Energies*, 2018, **11**, 3141.
- 109 M. C. Möller and S. Krauter, *Energies*, 2022, **15**, 2201.
- 110 M. C. Möller and S. Krauter, *Solar*, 2023, **3**, 25–48.
- 111 G. De Lorenzo, R. G. Agostino and P. Fragiaco, *Energies*, 2022, **15**, 6437.
- 112 S. Zhang, X. Hu, X. He, S. Tang, H. Li and D. Zhang, *Front. Energy Res.*, 2023, **11**, DOI: [10.3389/fenrg.2023.1209845](https://doi.org/10.3389/fenrg.2023.1209845).
- 113 I. Saedi, S. Mhanna and P. Mancarella, *Appl. Energy*, 2021, **303**, 117598.
- 114 G. Pan, W. Gu, Y. Lu, H. Qiu, S. Lu and S. Yao, *IEEE Trans. Sustain. Energy*, 2020, **11**, 2662–2676.
- 115 S. Boulmrharj, M. Khaidar, M. Bakhouya, R. Ouladsine, M. Siniti and K. Zine-dine, *Sustainability*, 2020, **12**, 4832.
- 116 G. Fan, B. Yang, P. Guo, S. Lin, S. G. Farkoush and N. Afshar, *Int. J. Hydrogen Energy*, 2021, **46**, 33718–33737.
- 117 C. Ceylan and Y. Devrim, *Int. J. Hydrogen Energy*, 2021, **46**, 22092–22106.
- 118 T. Hai, H. A. Dhahad, K. Sharma, S. Mehrez, A. Abdelrahman, S. F. Almojil, A. I. Almohana, A. F. Alali and A. G. Mohammed, *Sustain. Energy Technol. Assessments*, 2022, **54**, 102719.
- 119 S. M. Alirahmi, E. Assareh, A. Chitsaz, S. Ghazanfari Holagh and S. Jalilinasrabad, *Int. J. Hydrogen Energy*, 2021, **46**, 25650–25665.
- 120 A. C. Fărcaș, V. Sita, P. Dobra and R. Tîrnovan, *IFAC Proc. Vol.*, 2013, **46**, 32–36.
- 121 M. Rostami, M. D. Manshadi and E. Afshari, *J. Energy Storage*, 2022, **47**, 103635.
- 122 F. Gonzatti and F. A. Farret, *Energy Convers. Manag.*, 2017, **132**, 241–250.
- 123 A. Ganguly, D. Misra and S. Ghosh, *Energy Build.*, 2010, **42**, 2036–2043.
- 124 N. Yelegen, B. Kümük, R. N. Kaplan, M. İlbaş and Y. Kaplan, *Int. J. Hydrogen Energy*, 2023, **48**, 12969–12981.
- 125 H. Tao, K. Al Mamun, A. Ali, E. Solomin, J. Zhou and N. Sinaga, *Int. J. Hydrogen Energy*, 2024, **51**, 1280–1292.
- 126 Z. Mohammadi, P. Ahmadi and M. Ashjaee, *Energy*, 2023, **277**, 127352.
- 127 A. Chadly, E. Azar, M. Maalouf and A. Mayyas, *Energy*, 2022, **247**, 123466.
- 128 W. Sun, L. Feng, A. M. Abed, A. Sharma and A. Arsalanloo, *Energy*, 2022, **260**, 124947.
- 129 F. Calise, G. Ferruzzi and L. Vanoli, *Energy*, 2012, **41**, 18–30.
- 130 M. Persson, D. Mignard and D. Hogg, *Int. J. Hydrogen Energy*, 2020, **45**, 31396–31409.
- 131 S. Boulmrharj, M. Khaidar, M. Bakhouya, R. Ouladsine, M. Siniti and K. Zine-dine, *Sustainability*, 2020, **12**, 4832.
- 132 A. Chitsaz, M. A. Haghighi and J. Hosseinpour, *Energy Convers. Manag.*, 2019, **186**, 487–499.
- 133 F. Calise, R. D. Figaj, N. Massarotti, A. Mauro and L. Vanoli, *Appl. Energy*, 2017, **192**, 530–542.
- 134 Y. Kalinci, I. Dincer and A. Hepbasli, *Int. J. Hydrogen Energy*, 2017, **42**, 2492–2503.
- 135 A. Alobaid and R. A. Adomaitis, *Sustain. Energy Fuels*, 2023, **7**, 1395–1414.
- 136 S. L. Chavan and D. B. Talange, *J. Energy Storage*, 2018, **18**, 327–332.
- 137 F. J. Folgado, I. González and A. J. Calderón, *J. Energy Storage*, 2024, **75**, 109694.
- 138 A. Rajan, A. Garg, V. Vijayaraghavan, Y. C. Kuang and M. P.-L. Ooi, *J. Energy Storage*, 2018, **15**, 8–16.
- 139 M. Genovese and P. Fragiaco, *Int. J. Hydrogen Energy*, 2022, **47**, 12264–12280.
- 140 E. Crespi, P. Colbertaldo, G. Guandalini and S. Campanari, *J. Energy Storage*, 2022, **55**, 105613.
- 141 M. B. Hossain, M. R. Islam, K. M. Muttaqi, D. Sutanto and A. P. Agalgaonkar, *J. Energy Storage*, 2023, **62**, 106842.
- 142 H. Chen, H. Liu, M. Chen and H. Wang, *Fuel*, 2024, **365**, 131253.
- 143 H. J. Lim, G. Kim and G. J. Yun, *ACS Appl. Mater. Interfaces*, 2023, **15**, 24257–24270.
- 144 S. Chen, M. Hao, Y. Hu, K. Liu and Y. Li, *J. Power Sources*, 2024, **599**, 234238.
- 145 D. Madhav, J. Wang, R. Keloth, J. Mus, F. Buysschaert and V. Vandeginste, *Energies*, 2024, **17**, 998.
- 146 S. J. C. Cleghorn, D. K. Mayfield, D. A. Moore, J. C. Moore, G. Rusch, T. W. Sherman, N. T. Sisofo and U. Beuscher, *J. Power Sources*, 2006, **158**, 446–454.
- 147 K. Bareiß, C. de la Rua, M. Möckl and T. Hamacher, *Appl. Energy*, 2019, **237**, 862–872.
- 148 M. Zhang, H. Lv, H. Kang, W. Zhou and C. Zhang, *Int. J. Hydrogen Energy*, 2019, **44**, 25777–25799.
- 149 L. Tong, C. Yuan, T. Yang, Y. Yuan, R. Chahine and J. Xiao, *Case Stud. Therm. Eng.*, 2023, **43**, 102812.
- 150 M. A. Hossain, M. R. Islam, M. A. Hossain and M. J. Hossain, *J. Energy Storage*, 2023, **72**, 108170.
- 151 T. Egeland-Eriksen, A. Hajizadeh and S. Sartori, *Int. J. Hydrogen Energy*, 2021, **46**, 31963–31983.
- 152 M. Kopp, D. Coleman, C. Stiller, K. Scheffer, J. Aichinger and B. Scheppat, *Int. J. Hydrogen Energy*, 2017, **42**, 13311–13320.
- 153 M. Yue, H. Lambert, E. Pahon, R. Roche, S. Jemei and D. Hissel, *Renew. Sustain. Energy Rev.*, 2021, **146**, 111180.
- 154 C. Lubritto, in *Trends in Telecommunications Technologies*, InTech, 2010.



- 155 N. R. Devela, T. C. Kandpal and B. Singh, *Environ. Dev. Sustain.*, 2023, **26**, 2897–2964.
- 156 S. Cordiner, V. Mulone, A. Giordani, M. Savino, G. Tomarchio, T. Malkow, G. Tsotridis, A. Pilenga, M. L. Karlsen and J. Jensen, *Appl. Energy*, 2017, **192**, 508–518.
- 157 L. Bartolucci, S. Cordiner, V. Mulone and S. Pasquale, *Appl. Energy*, 2019, **252**, 113386.
- 158 P. Aliberti, M. Sorrentino, M. Califano, C. Pianese, L. Capozucca, L. Cristiani, G. Lops and R. Mancini, *Energies*, 2023, **16**, 6316.
- 159 Z. Zhang, K. Sato, Y. Nagasaki, M. Tsuda, D. Miyagi, T. Komagome, K. Tsukada, T. Hamajima, Y. Ishii and D. Yonekura, *Int. J. Hydrogen Energy*, 2019, **44**, 23384–23395.
- 160 S. T. Le, T. N. Nguyen, D.-K. Bui, B. Teodosio and T. D. Ngo, *Energy*, 2024, **290**, 130041.
- 161 A. M. Elberry, J. Thakur and J. Veysey, *J. Energy Storage*, 2021, **44**, 103474.
- 162 Á. Hernández-Gómez, V. Ramirez, D. Guilbert and B. Saldivar, *Membranes*, 2021, **11**, 379.
- 163 L. Pilon, H. Wang and A. d'Entremont, *J. Electrochem. Soc.*, 2015, **162**, A5158–A5178.
- 164 C. Immerz, B. Bensmann, P. Trinke, M. Suermann and R. Hanke-Rauschenbach, *J. Electrochem. Soc.*, 2019, **166**, F1200–F1208.
- 165 F. Grumm, M. Schumann, C. Cosse, M. Plenz, A. Lücken and D. Schulz, *Electronics*, 2020, **9**, 602.
- 166 J. P. Sabawa and A. S. Bandarenka, *Results Chem.*, 2020, **2**, 100078.
- 167 D. Guilbert, B. Yodwong, W. Kaewmanee, M. Phattanasak and M. Hinaje, Hydrogen Flow Rate Control of a Proton Exchange Membrane Electrolyzer, in *Proceedings of the 2019 Research, Invention, and Innovation Congress (RI2C)*, Bangkok, Thailand, 2019.
- 168 D. D. Nation and K. L. Smith, *Modelling the Dynamics of a Polymer Electrolyte Membrane (PEM) Electrolyser at Start-Up*, 2016.
- 169 D. Guilbert, D. Sorbera and G. Vitale, *Int. J. Hydrogen Energy*, 2020, **45**, 64–79.
- 170 A. M. Dhirde, N. V. Dale, H. Salehfar, M. D. Mann and T.-H. Han, *IEEE Trans. Energy Convers.*, 2010, **25**, 778–786.
- 171 D. Guilbert and G. Vitale, *Energies*, 2019, **12**, 750.
- 172 Á. Hernández-Gómez, V. Ramirez, D. Guilbert and B. Saldivar, *Int. J. Hydrogen Energy*, 2020, **45**, 18817–18830.
- 173 S. S. Mohammadshahi, E. M. A. Gray and C. J. Webb, *Int. J. Hydrogen Energy*, 2016, **41**, 3470–3484.
- 174 A. Jemni, *Int. J. Hydrogen Energy*, 1995, **20**, 881–891.
- 175 A. Jemni, *Int. J. Hydrogen Energy*, 1995, **20**, 43–52.
- 176 S. Nasrallah, *Int. J. Hydrogen Energy*, 1997, **22**, 67–76.
- 177 M. L. Moropeng, A. Kolesnikov, M. Lototsky and A. Mavhungu, *Chem. Prod. Process Model.*, 2019, **14**(3), DOI: [10.1515/cppm-2018-0050](https://doi.org/10.1515/cppm-2018-0050).
- 178 J. R. Lacher, *Proc. R. Soc. London, Ser. A*, 1937, **161**, 525–545.
- 179 H. A. Kierstead, *J. Less-Common Met.*, 1980, **71**, 303–309.
- 180 M. V. Lototsky, *Int. J. Hydrogen Energy*, 2016, **41**, 2739–2761.
- 181 B. J. Hardy and D. L. Anton, *Int. J. Hydrogen Energy*, 2009, **34**, 2269–2277.
- 182 B. J. Hardy and D. L. Anton, *Int. J. Hydrogen Energy*, 2009, **34**, 2992–3004.
- 183 S. N. Nyamsi, F. Yang and Z. Zhang, *Int. J. Hydrogen Energy*, 2012, **37**, 16078–16092.
- 184 A. Aghakhani, N. Haque, C. Saccani, M. Pellegrini and A. Guzzini, *Int. J. Hydrogen Energy*, 2023, **48**, 30170–30190.
- 185 Facts on Climate Change, How are CO₂ concentrations related to warming?, <https://factsonclimate.org/infographics/concentration-warming-relationship#sources-and-notes>, (accessed 6 September 2024).
- 186 S. C. Sherwood, M. J. Webb, J. D. Annan, K. C. Armour, P. M. Forster, J. C. Hargreaves, G. Hegerl, S. A. Klein, K. D. Marvel, E. J. Rohling, M. Watanabe, T. Andrews, P. Braconnot, C. S. Bretherton, G. L. Foster, Z. Hausfather, A. S. von der Heydt, R. Knutti, T. Mauritsen, J. R. Norris, C. Proistosescu, M. Rugenstein, G. A. Schmidt, K. B. Tokarska and M. D. Zelinka, *Rev. Geophys.*, 2020, **58**(4), DOI: [10.1029/2019RG000678](https://doi.org/10.1029/2019RG000678).
- 187 S. Ferrarese, Upgrade e commissioning di un sistema di test ad alte prestazioni per celle a combustibile di tipo PEM, Master thesis, Università degli studi di Padova, 2013.
- 188 P. Thounthong, P. Tricoli and B. Davat, *Int. J. Electr. Power Energy Syst.*, 2014, **54**, 454–464.
- 189 P. Millet, R. Ngameni, S. A. Grigoriev, N. Mbemba, F. Brisset, A. Ranjbari and C. Etiévant, *Int. J. Hydrogen Energy*, 2010, **35**, 5043–5052.
- 190 M. Shen, N. Bennett, Y. Ding and K. Scott, *Int. J. Hydrogen Energy*, 2011, **36**, 14335–14341.
- 191 A. Farsi and M. A. Rosen, *e-Prime - Adv. Electr. Eng. Electron. Energy*, 2023, **4**, 100174.
- 192 A. María Villarreal Vives, R. Wang, S. Roy and A. Smallbone, *Appl. Energy*, 2023, **346**, 121333.
- 193 O. Corigliano, M. Genovese and P. Fragiaco, *J. Power Sources*, 2025, **629**, 236076.
- 194 F. S. Mahmoud, A. M. Abdelhamid, A. Al Sumaiti, A.-H. M. El-Sayed and A. A. Z. Diab, *Mathematics*, 2022, **10**, 3708.
- 195 ISPRA, *Fattori di emissione per la produzione ed il consumo di energia elettrica in Italia*, 2024.

